Control concepts for power reference tracking

Deliverable 3.1

Grant Agreement No.	883553
Start date of Project	1 April 2020
Duration of Project	48 months
Deliverable Number	D3.1
Deliverable Leader	Ghent University
Dissemination Level	Public
Version	V1.0
Submission Date	31-03-2021
Author(s)	Daan Truijen (Daan.Truijen@UGent.be) Jeroen De Kooning (Jeroen.DeKooning@UGent.be)

This project has received funding from the European Union's Horizon 2020 research and innovation programme under grant agreement No 883553.

Modification Control

Version #	Description	Author	Organisation	Date
0.1	First draft	Daan Truijen, Jeroen de Kooning	Ghent University	16-03-2021
0.2	Second draft	Daan Truijen, Jeroen de Kooning	Ghent University	26-03-2021
1.0	Final version	Daan Truijen, Jeroen de Kooning	Ghent University	30-03-2021

Release Approval

Name	Role	Date
Jeroen De Kooning	WP Leader	30-03-2021
Jeremy Bricker	Technical Project Coordinator	30-03-2021
Roelof Moll	Executive Project Coordinator	31-03-2021

Preface

With the increasing penetration of renewable energy sources in the pan-European grid, their fluctuating and intermittent nature hinders grid stability. Therefore, there is an increased need for flexible energy storage systems. Grid stability can be augmented and maintained by implementing pumped hydropower energy storage. This is a technology that has proven to be economically viable because of its long lifespan. However, not all sites have the natural topography needed for the conventional setups. Therefore, ALPHEUS will improve Reversible Pump-Turbine (RPT) and corresponding technologies for sites with a relatively flat topography. The RPT designs comprise two contra-rotating RPTs and a positive displacement RPT. In the contra-rotating concepts, two runners (propellers) rotate in opposite direction to reduce swirl and increase efficiency. Within ALPHEUS, Work Package 3 investigates the Power Take-Off (PTO) and machine-side control. The PTO comprises the electric machines, machine components and transmission shafts. For the contra-rotating RPT concepts, the two runners are separately driven by two electric machines, to ensure operating at the optimal operating point. For the machine-side control, it will be investigated how the runners and inlet vanes have to be controlled to satisfy grid needs. In this deliverable, control concepts are discussed, which have an optimal dynamic, efficient and precise response to a power setpoint from the grid.

Contents

Nomenclature

A Surface covered by RPT [m^2]

Ch Variable describing h vs. Q [s/m^5]

Cp Variable describing P vs. Q [/]

Ct Variable describing T vs. Q [m]

e Mean height of pipe imperfection [m]

D Diameter of pipe system [m]

F Rotational friction

f Friction factor for major losses

h Head (or pressure expressed as equivalent head) [m]

$\Delta h = h_1 - h_2$ Head height between reservoirs [m]

h_L Head loss [m]

i Current [A]

J Rotational moment of inertia [kg m^2]

k Minor loss coefficient [/]

k_c Loss coefficient describing permanent major & minor loss coefficient [/]

$k_v(\alpha)$ Minor loss coefficient of inlet vanes [/]

L Length of a pipe [m]

L_d,L_q d axis inductance, q axis inductance [H]

N_p Number of pole pairs [/]

$\dot{m}$ Mass flow rate [kg/s]

P Pump power [W]

p Absolute pressure [Pa]

Q Flow rate [m^3/s]

Re Reynolds number [/]

T_m Electrical machine torque [Nm]

T_r Rotor (load) torque [Nm]

v Linear flow speed [m/s]

v voltage [V]

α Inlet vanes angle or setting, between 0 and 1 [/]

η Efficiency [%]

λ Tip Speed Ratio [rpm s]

Ω Rotational speed of propeller in [rpm]

ψ_{PM} Flux of the permanent magnets [Wb]

ρ Material density [kg/m^3]

ζ Speed ratio $\frac{\Omega_2}{\Omega_1}$ [/]

Executive Summary

This report describes control concepts for power reference tracking. The goal is to find an algorithm that drives the two Reversible Pump-Turbine (RPT) runners and the inlet vanes to reach a power setpoint, based on grid state, optimally fast, efficient and precise. First, explicit relations for RPT power, RPT head and runner torques versus flow rate and rotational speed of the first runner are found in both operating modes for an initial shaft-driven Contra-Rotating (CR) RPT. Next, a static water model is constructed. This model calculates the flow rate and runner torques for given rotational speeds of the runners and a given inlet vane angle. In a next stage, it is presented how flow rate and RPT power change as a function of the runner speeds and inlet vane angle, again for both operating modes. Now, it can be found how the RPT needs to be controlled to reach a desired power setpoint, with a certain system head height.

The machine-side control is split into the high level and low level control. The low level control controls the electric machine currents, to reach the torque setpoints, using vector control or field oriented control. In vector control, the currents in the rotating frame, found through the Clarke-Park transformation, are regulated as constant values, proportional to the torque setpoint. These torque setpoints are outputs from the high level control, which are found based on the power setpoints from the grid and current system state. For both operating modes, high level control concepts are proposed that use one, two or three of the three available control parameters. As mentioned, these control parameters comprise both runner speeds and the inlet vane angle. For the single variable control system, the inlet vanes are only used for startup and stop methods and the second runner is driven to always reach the design speed ratio of 90% of the first runner speed. It is found that in turbine mode, a robust Perturb & Observe (P&O) algorithm can be used. The main advantage of this algorithm is its viability for unknown and changing system parameters. However, P&O is inherently slow. In pump mode, a lookup table can be used that stores the rotational speed that corresponds with the current head height between the water reservoirs and the power setpoint. These values are stored in the table based on calculated or measured values. When lookup tables are used, a superposed P&O algorithm can be added to make small increments to the rotational speed, to reach the optimal power setpoint precisely. This is necessary because of small errors in the tabulated data which are unavoidable. These inaccuracies include measurement errors of the head height, errors in estimations of the major and minor losses and interpolation errors between the stored points in the lookup table.

Although a single variable control algorithm can work, using the inlet vane angle as a second control parameter has a significant advantage. Since reservoir capacity is limited and under-frequency in the pan-European grid is more common than over-frequency (and the system will thus be used more in turbining mode),

it can be useful to reach the power setpoint in turbine mode with the lowest possible flow rate. It is found that for a certain power setpoint, an infinite amount of combinations between the inlet vane angle and the first runner speed exist, which operate at different flow rates. Therefore, a lookup table can be used that stores the combination for inlet vane angle and first runner speed, where the flow rate is minimal for a certain head height and power setpoint. The same applies in pump mode, although it is more likely that the system will operate at the highest flow rate (and thus with open inlet vanes), for the same reason as listed above.

Next, the influence of varying the speed ratio from the design speed ratio is elaborated on. It is found that the lookup tables described above can also be made for a weighted mean rotational speed, instead as for the first runner speed. Doing this results in two main benefits. First, the system is more dynamic, since the first runner has a lower moment of inertia. Therefore, the first runner can accelerate or decelerate more quickly to reach the mean rotational speed faster. Secondly, the rotational speeds can be chosen to distribute the runner power evenly, while maintaining the same total power.

Since the main document focuses on results of the CR RPT CFD calculations, the differences in approach are listed for the Positive Displacement (PD) RPT. Here, a significantly small gap is present between the two runners. Therefore, the relative position between the runners must always be ensured. If the relative position control is executed electrically (i.e. the runners are actuated by two separate electrical machines), a master slave control is used. Here, the first runner is speed controlled, based on the power setpoint and power controller, while the second runner's torque is controlled to keep the relative angle between both lobes constant. With the limited CFD results available, it is discussed that the high level control concepts, described above, are also applicable for the PD RPT, with the exception of the varying speed ratio. However, this will be confirmed in future work.

1 Introduction

This deliverable describes the control concepts for power reference tracking of three Reversible Pump-Turbine (RPT) types, that are studied in work package 2 of the H2020 ALPHEUS project. These comprise a Contra-Rotating (CR) shaft-driven RPT, a CR rim-driven RPT and a Positive Displacement (PD) RPT. CFD calculations are available and are analysed in this deliverable for the shaft-driven CR RPT. Since the rim-driven CR RPT will have similar characteristics, the control concepts developed for the shaft-driven CR RPT are applicable on the rim-driven CR RPT as well. The deliverable's main focus includes describing how the different control parameters can be managed and driven to achieve a system that has an optimally precise, dynamic and efficient response to a given variable power setpoint from the grid. The control parameters comprise the machine torques and inlet vane angle. Since blade pitch has not been implemented in WP2, it is not described here. However, it can still be part of future research.

This document is structured as follows: In section 2, the control system is described. Furthermore, this section also described how the real system will be modelled to get initial results from calculations and simulations. In section 3, the CFD calculations for the shaft-driven CR RPT are analysed for a fixed ratio of the two rotor speeds. These CFD calculations include how power, head and runner torques change with variable speed and flow rate. By using curve fitting on these data points, the RPT and its characteristics can be described. However, a control system should not only take into account the RPT curves. Therefore, in section 4, a static water flow model is constructed. This water flow model calculates the flow rate for given rotational speeds of the RPT, combined with system parameters, such as inlet vane angle and head height of the reservoirs. From this flow rate, the water flow model calculates the runner torques. In section 5, it is described how the electrical machine needs to be driven to reach a desired torque setpoint. In section 6, the conceptual control systems are described, which in turn will drive the electrical machines and inlet vane angle. In section 7, it is described how using a variable speed ratio control can optimize the machine side control system. Finally in section 8, the differences in approach for the Positive Displacement RPT are listed.

Note that this deliverable works with a preliminary and limited dataset. Therefore, the developed curves and control systems are conceptual and aim to give an overview of how the RPT and system behaves, as well as to how the different control parameters can be used to reach a certain power setpoint fast, efficiently and robustly. In future research, detailed control systems will be designed based on the concepts described in this deliverable. This future research also includes a full multi-dimensional Model-based Predictive Control (MPC) system (cfr. Task 3.5) and a more detailed approach to defining a difference between synthetic inertia, primary response and secondary response.

2 Machine side model overview

Fig. 1 schematically visualises the machine side control system for the two runners in the shaft-driven CR RPT. The high level control decides, based on measured values and the control algorithm, what its output setpoints are. These setpoints comprise the torques for both runners and the inlet vane angle. The torque setpoints are sent to the low level control, that determines the switching signals for the power electronic converters to realize these torque setpoints. The low level control is explained further in section 5. Note that in some control systems, the low level control includes a cascaded control, where it receives a rotational speed setpoint from the high level control. This will also be explained in the section.

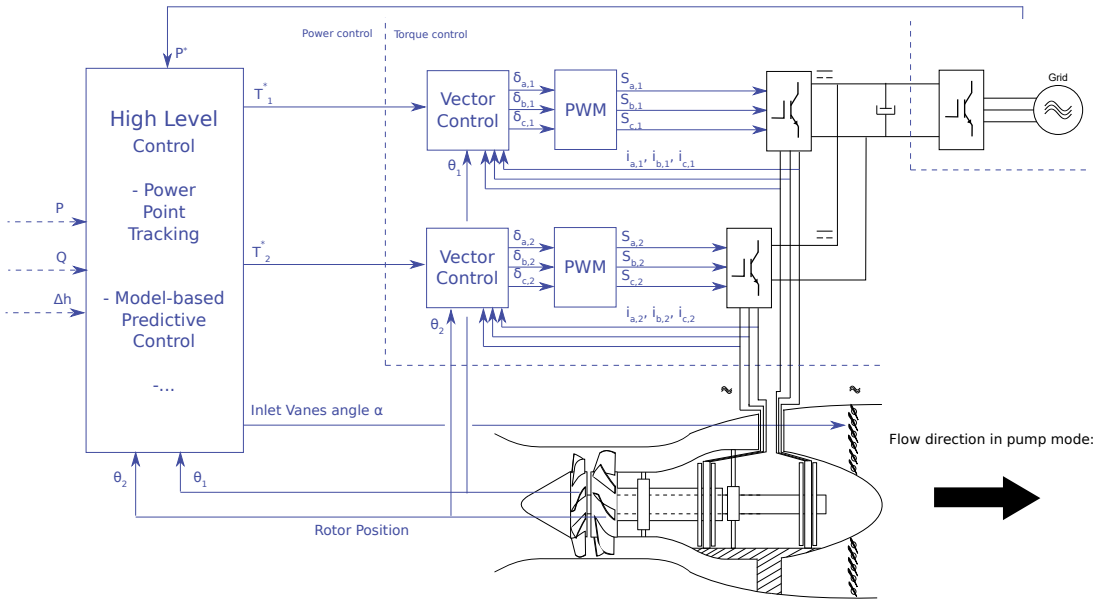

Figure 1: Control schematic

Fig. 2 shows how the system is modelled and how this model is structured. The system is divided into two blocks: the water model and the motor model including mechanical dynamics. The motor model outputs the two machine torques T_m, based on given inverter outputs of the low level control. The water model, discussed in section 4, calculates runner torques T_r. It does this by calculating the flow rate Q based on the head height Δh between the two basins, the inlet vane angle α and the rotational speeds of the runners Ω_1, Ω_2. Based on the flow rate Q, the runner torques can then be calculated, based on the CFD curves, discussed in section 3. The mechanical dynamics calculate the runner speeds

based on the two interacting torque values.

$$T_{r1} - T_{m1} = J_{r1}\frac{d\Omega_1}{dt} + F\ \Omega_1 \tag{1}$$

$$T_{r2} - T_{m2} = J_{r2}\frac{d\Omega_2}{dt} + F\ \Omega_2 \tag{2}$$

Here, T_{r1} and T_{r2} are the respective torques of the runners, while T_{m1} and T_{m2} are the respective torques of the electrical machines. J_{r1} is the combined moment of inertia of runner 1, the transmission shaft and the electrical machine 1. J_{r2} is the combined inertia for the second rotor. F is the friction coefficient, which can be nonlinear, i.e., speed dependent. Note that $J_{r1} < J_{r2}$.

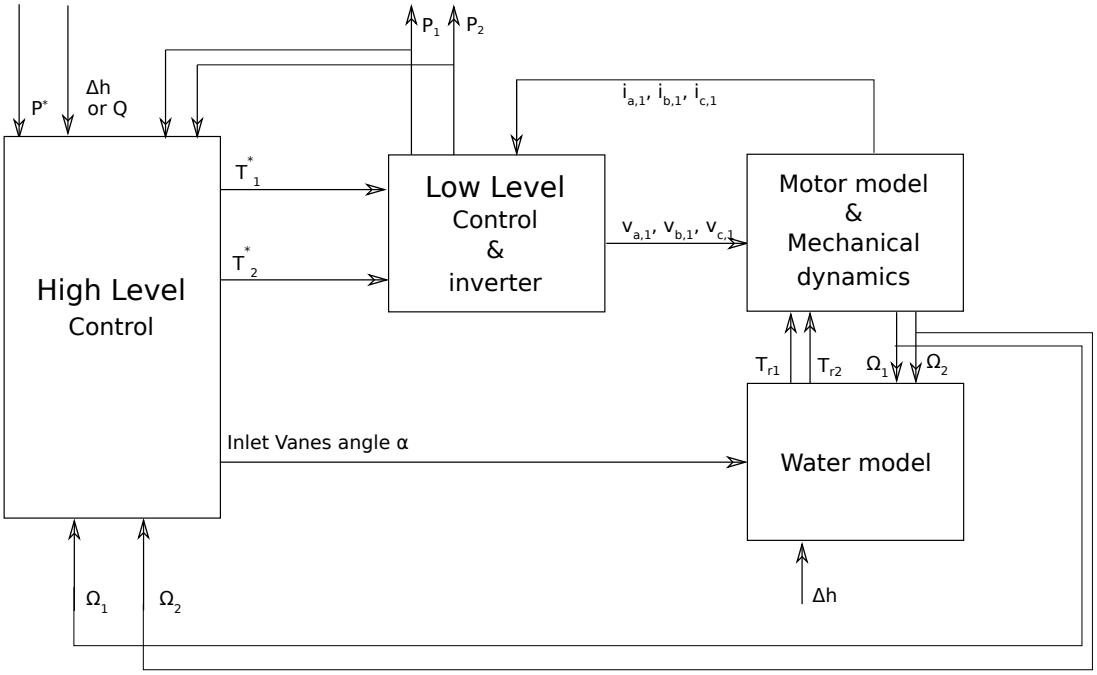

Figure 2: Control schematic model

3 CFD Curves

For the initial control system evaluation, CFD calculations were performed in WP2 at multiple steady state operating points at variable rotational speed and variable flow rate for both pump & turbine modes. The output of these calculations included mechanical power, efficiency and head for both runners separately and combined, as well as torque and axial force for both runners. In a first stage, a wide range of operating points was simulated in Ansys. From this data, the operating range could be narrowed down and more simulations were performed in OpenFOAM. As will be seen throughout this section, both simulation platforms have generated similar results for most output parameters. The exception to this is head and efficiency for sub-nominal rotational speed in turbine mode.

With these data, it can be analysed how power P, head H and torque T change with regard to the rotational speeds Ω_1 and Ω_2, for different flow rates Q. For the control system, the output parameters that must be known over the full operating range are:

- Total RPT power $P_{\mathrm{RPT}}(Q, \Omega_1, \Omega_2)$
- Total RPT head $H_{\mathrm{RPT}}(Q, \Omega_1, \Omega_2)$
- Runner torques $T_{r1}(Q, \Omega_1, \Omega_2)$, $T_{r2}(Q, \Omega_1, \Omega_2)$

In this section, polynomial regression curves will be determined corresponding with the calculated datapoints for the output parameters. The goal is to find a common curve for all different flow rates, so that a common equation is found between the output parameter (e.g. P_{RPT}) and the input parameters Ω_1 and Q. Important to note, is that the rotational speed Ω will be represented with the unit rpm throughout this deliverable to increase interpretability for the reader. First, the speed ratio is kept constant at $\Omega_2 = 0.9 \cdot \Omega_1$, which is the design speed ratio and optimal at nominal speeds and flow rate. In section 7, it is discussed how altering this ratio affects the RPT.

3.1 Turbine mode

3.1.1 Total turbine power

Fig. 3 shows total power P_{RPT} versus rotational speed Ω_1 for three different flow rates. For each flow rate, the unstable operating points are represented in a different color. In the control system, these points are avoided. It can be seen that for all flow rates, the curve has the same form. Furthermore, it can be seen that P_{RPT} is greater for higher flow rates. Next, the speed Ω_1, for which P_{RPT} is maximal, increases with increasing flow rate.

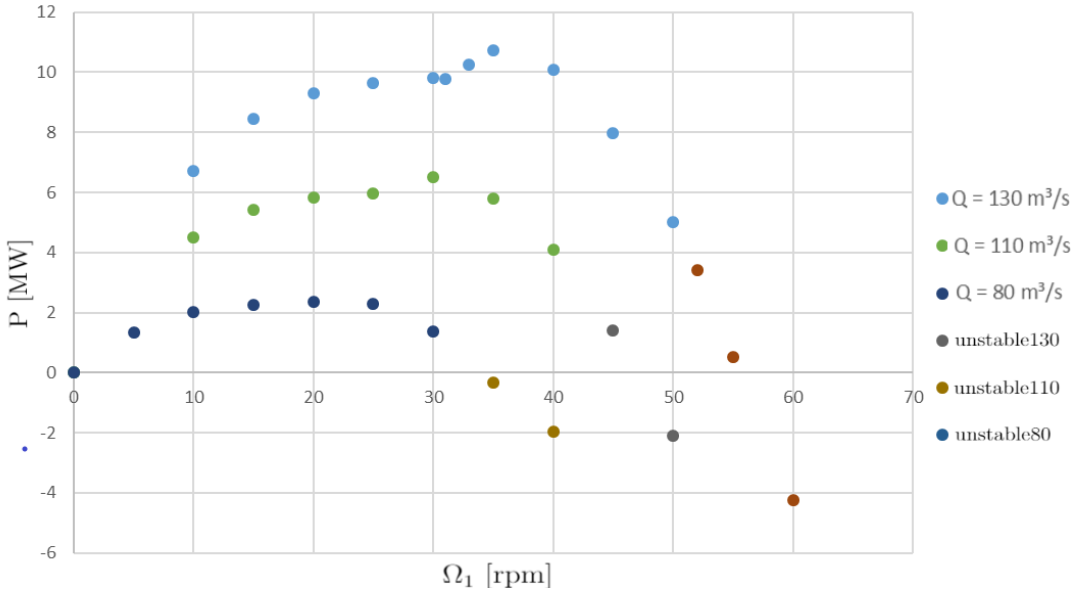

Figure 3: P vs. Ω_1 for different flow rates Q [m^3/s]

The results described above are something that is also seen in wind turbines. In wind turbines, the Tip Speed Ratio (TSR) λ is introduced as a dimensionless parameter representing the ratio between rotational speed and wind speed. Here, the TSR λ is defined as:

$$\lambda = \frac{\Omega_1 \ R \ A}{Q} \tag{3}$$

As can be seen in Fig. 4, plotting P versus a TSR λ, results in an optimal TSR, for which every flow rate produces the maximal amount of power. It can also be seen that unstable operation starts at comparable TSR for all flow rates. Now, Cp is introduced to make a generalized curve, visualised in Fig. 5. Cp is a dimensionless variable, but has no real physical interpretation.

$$Cp = \frac{P_{\text{RPT}}}{0.5 \ \rho \ Q^3/A^2} \tag{4}$$

It can be seen that for all flow rates, there is a common relation between Cp and λ. This relation can be defined by curve fitting between the datapoints. This is done with the Matlab curve fitting tool. A 5th order polynomial curve fit has an R-square value of 0.9971 and Root Mean Square Error (RMSE) of 0.1911:

$$Cp = 1.836 \cdot 10^{-6} \ \lambda^5 - 0.0002048 \ \lambda^4 + 0.007861 \ \lambda^3 - 0.1425 \ \lambda^2 + 1.426 \ \lambda \tag{5}$$

A rational curve fit, with 5th order numerator and 2nd order denominator gives better results around the maximum point and reduces the error to an R-square

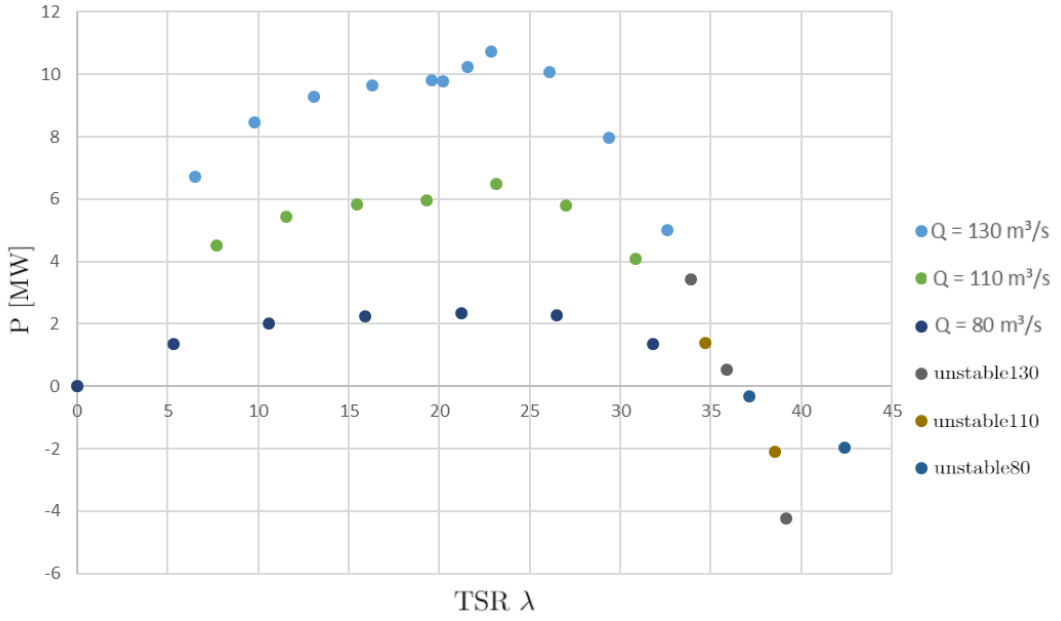

Figure 4: Total power P_{RPT} vs. TSR λ for different flow rates Q [m³/s]

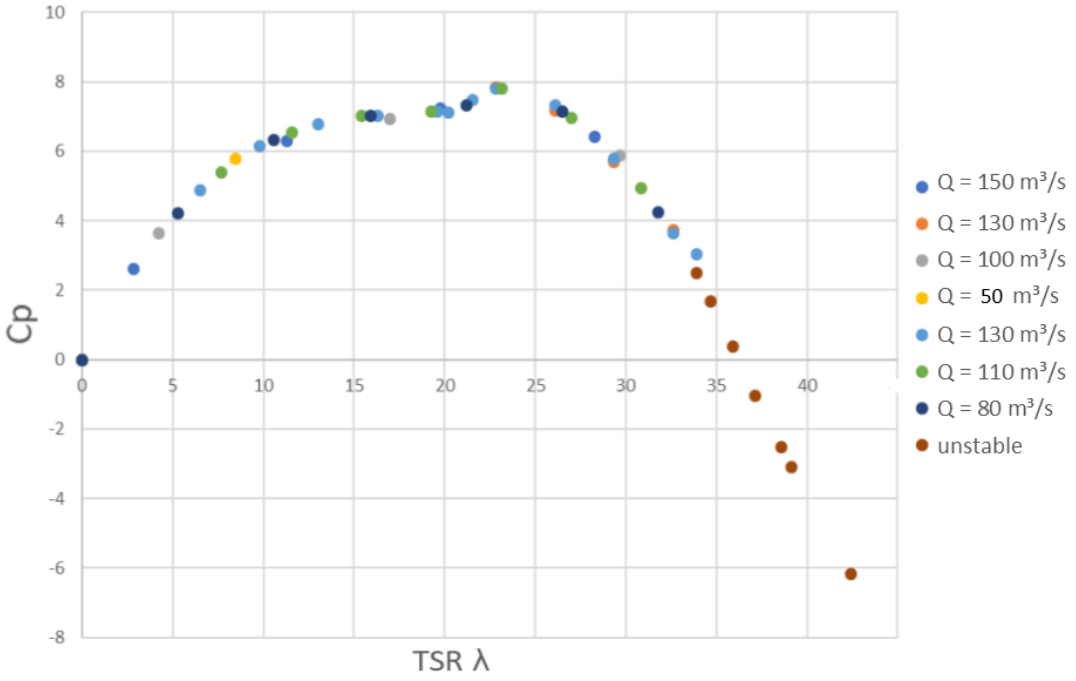

Figure 5: C_p versus TSR for different flow rates Q [m³/s]

value of 0.9993 and an RMSE of 0.09609:

$$Cp = \frac{8.34 \cdot 10^{-5}\ \lambda^5 - 0.03667\ \lambda^4 + 2.455\ \lambda^3 - 58.21\ \lambda^2 + 487.7\ \lambda - 0.258}{\lambda^2 - 41.63\ \lambda + 502.6} \quad (6)$$

For any given Ω_1 and Q, the total power P_{RPT} can be calculated from the given equations. Note that the stable operating range extends to a TSR of $\lambda = 32.5$.

3.1.2 Runner torques

For the runner torques, the same method is applied to find a common curve for all flow rates. $\mathrm{Ct_{R1}}$ and $\mathrm{Ct_{R2}}$ represent the torque of respectively runner 1 and runner 2 and can be defined by two 3rd order curve fits in function of TSR λ. Ct is expressed in [m] and defined here by:

$$Ct = \frac{T}{0.5\ \rho\ Q^2/A} \tag{7}$$

Fig. 6 and 7 show the data obtained from CFD simulations. Polynomial curve fits are applied on these data to obtain closed form formulations for the runner torque. Ct_{R1} is represented by a 3rd order polynomial curve with an R-square value of 0.9967 and RMSE of 0.2955.

$$Ct_{R1} = -0.0008781\ \lambda^3 + 0.05634\ \lambda^2 - 1.427\ \lambda + 17.7 \tag{8}$$

Ct_{R2} is represented by a 3rd order polynomial curve with an R-square value of 0.9964 and RMSE of 0.233. Note that λ_{r2} is the TSR of the second runner.

$$Ct_{R2} = -0.000255\ \lambda_{r2}^3 + 0.01762\ \lambda_{r2}^2 - 0.7175\ \lambda_{r2} + 15.36 \tag{9}$$

3.1.3 Total turbine head

As mentioned, the CFD calculations were performed in two parts, with two different CFD programs. While results are similar for C_p, $\mathrm{Ct_{r1}}$ and $\mathrm{Ct_{r2}}$, the results for efficiency and head differ for sub-nominal (low) rotational speeds, between both programs. In the simulation model created with this deliverable, the simulation points from openFOAM are used. However, it is important to locate the origin of this difference in the future. The total turbine head is defined by:

$$Ch_{\mathrm{RPT}} = \frac{h_{\mathrm{RPT}}}{Q^2} \tag{10}$$

Fig. 8 shows the simulated data obtained from CFD. The following polynomial curve fits are obtained: A 2nd order polynomial fit with an R-square value of 0.9866 and RMSE of $5.28 \cdot 10^{-5}$, and a 3rd order polynomial with a R-square value of 0.9977 and a RMSE of $2.247 \cdot 10^{-5}$.

$$Ch_{\mathrm{RPT}} = 5.067 \cdot 10^{-7}\ \lambda^2 - 6.567 \cdot 10^{-5}\ \lambda + 0.001825 \tag{11}$$

$$Ch_{\mathrm{RPT}} = -5.660 \cdot 10^{-8}\ \lambda^3 + 4.292 \cdot 10^{-6}\ \lambda^2 - 0.00014\ \lambda + 0.00222 \tag{12}$$

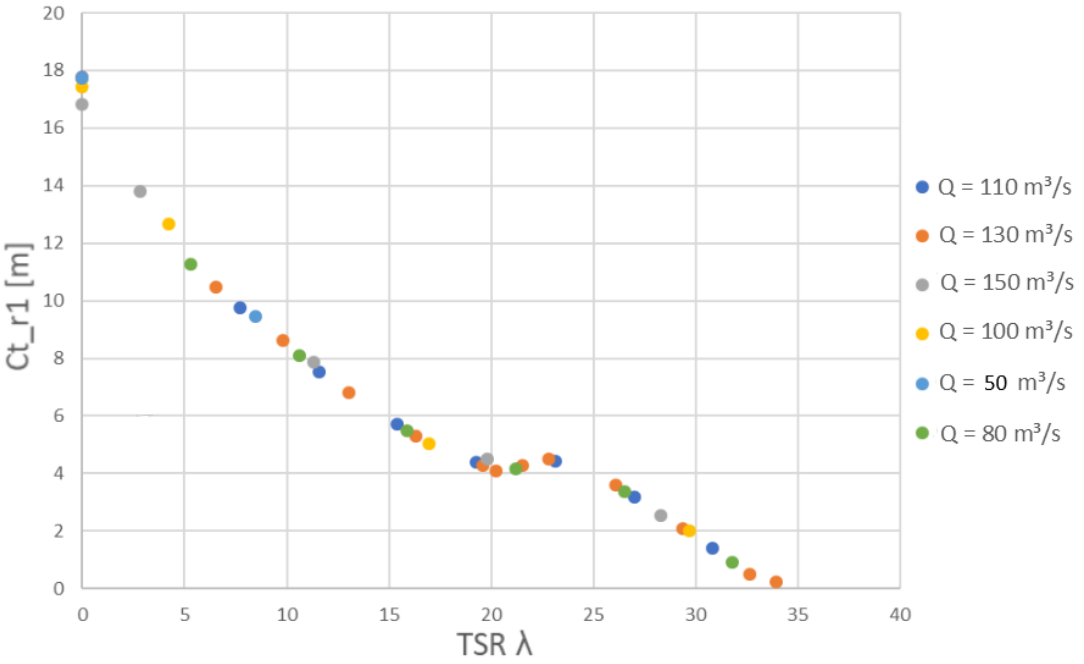

Figure 6: Ct_{R1} vs. TSR for different flow rates Q [m^3/s]

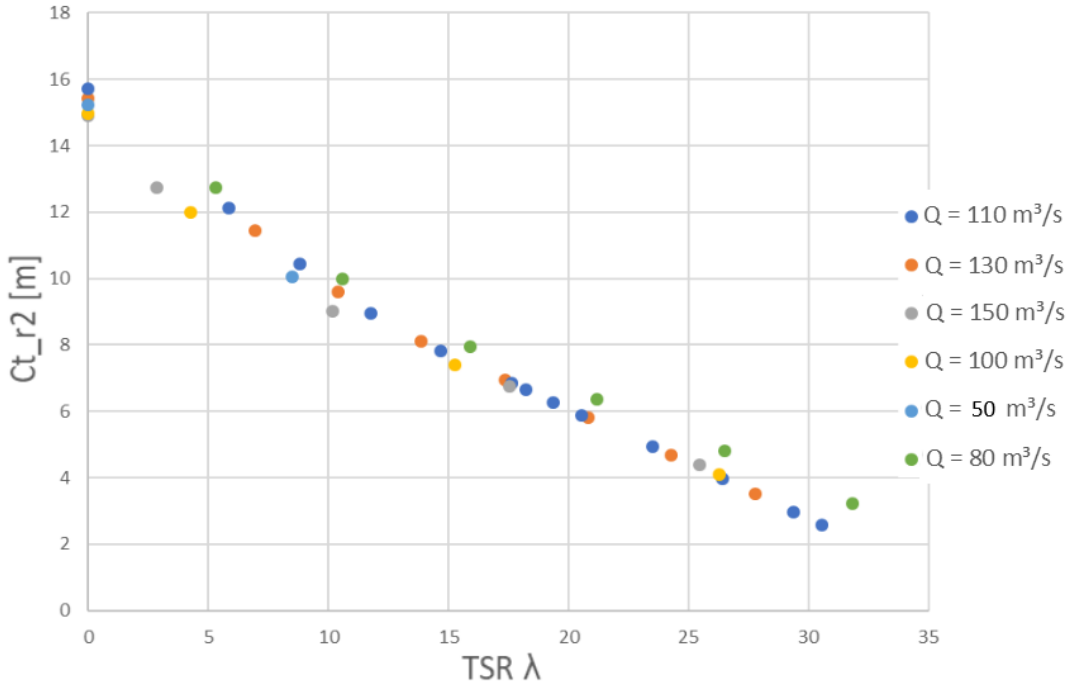

Figure 7: Ct_{R2} vs. TSR for different flow rates Q [m^3/s]

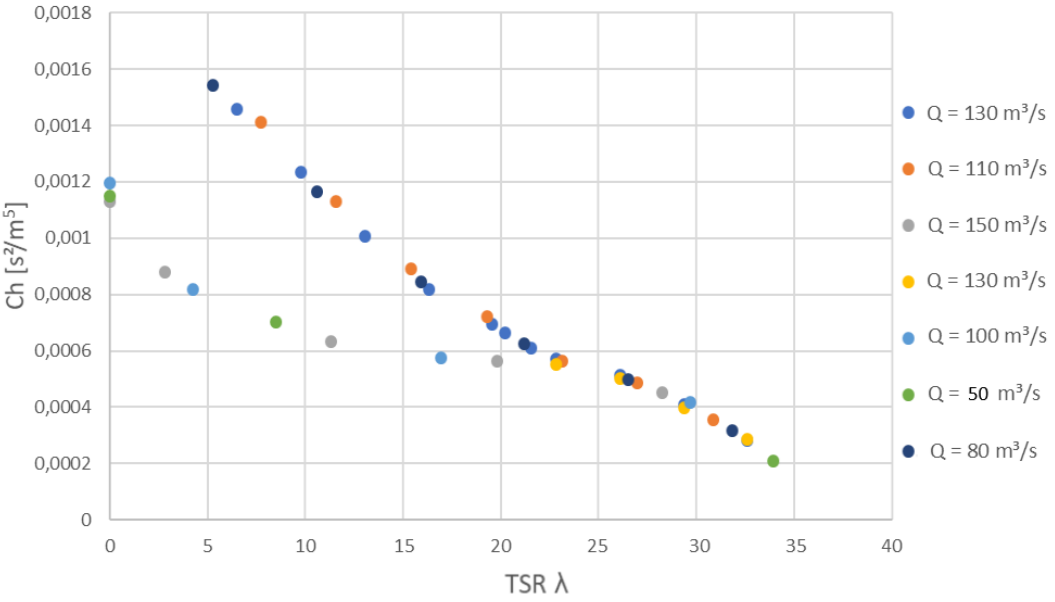

Figure 8: $\mathrm{Ch_{RPT}}$ vs. TSR for different flow rates Q [$\mathrm{m^3/s}$]

3.2 Pump mode

3.2.1 Total pump power

The power P is calculated using the dimensionless variable C_p, similarly as for turbine mode:

$$Cp = \frac{P_{\mathrm{RPT}}}{0.5\ \rho\ Q^3/A^2} \tag{13}$$

Fig. 9 illustrates C_p versus Ω_1 for different flow rates. Note that the RPT is unstable at low rotational speeds and thus low TSR. Therefore, it can be determined that the operating range of the RPT in pump mode must be greater than $\lambda = 30$. C_p can be represented by a 2nd order polynomial curve with an R-square value of 0.9988 and RMSE of 0.3773.

$$Cp = 0.01178 \cdot \lambda^2 - 0.08943 \cdot \lambda - 4.156 \tag{14}$$

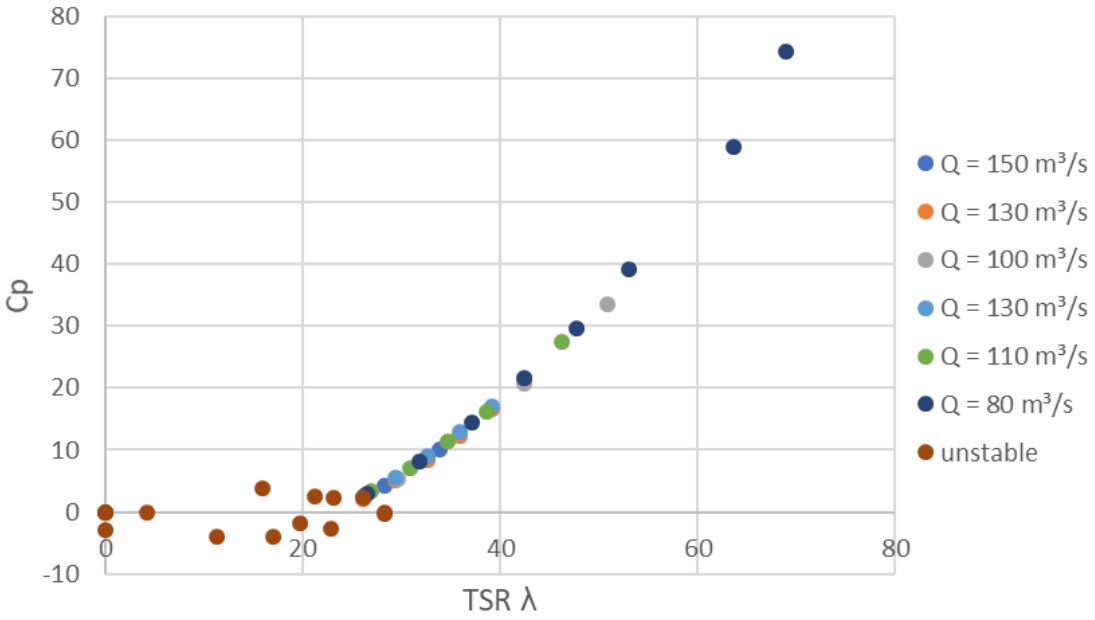

Figure 9: C_p vs. TSR for different flow rates Q [m³/s]

3.2.2 Runner torques

The torques T_{r1} and T_{r2} are represented by Ct, which is expressed in [m]. Figs. 10 and 11 illustrate Ct_{r1} and Ct_{r2} versus TSR for different flow rates. Note that again, Ct_{r2} is plotted versus the TSR of the second runner. Ct_{r1} is represented by a 4th order polynomial curve with an R-square value of 0.9947 and RMSE of

0.2095. Ct_{r2} is represented by a 4th order polynomial curve with an R-square value of 0.9963 and RMSE of 0.3231.

$$Ct = \frac{T}{0.5\ \rho\ Q^2/A} \tag{15}$$

$$Ct_{R1} = 3.18 \cdot 10^{-6}\ \lambda^4 - 0.0004446\ \lambda^3 + 0.0201\ \lambda^2 - 0.07066\ \lambda - 3.137 \tag{16}$$

$$Ct_{R1} = 9.06 \cdot 10^{-6}\ \lambda^4 - 0.00149\ \lambda^3 + 0.08478\ \lambda^2 - 1.453\ \lambda + 4.44 \tag{17}$$

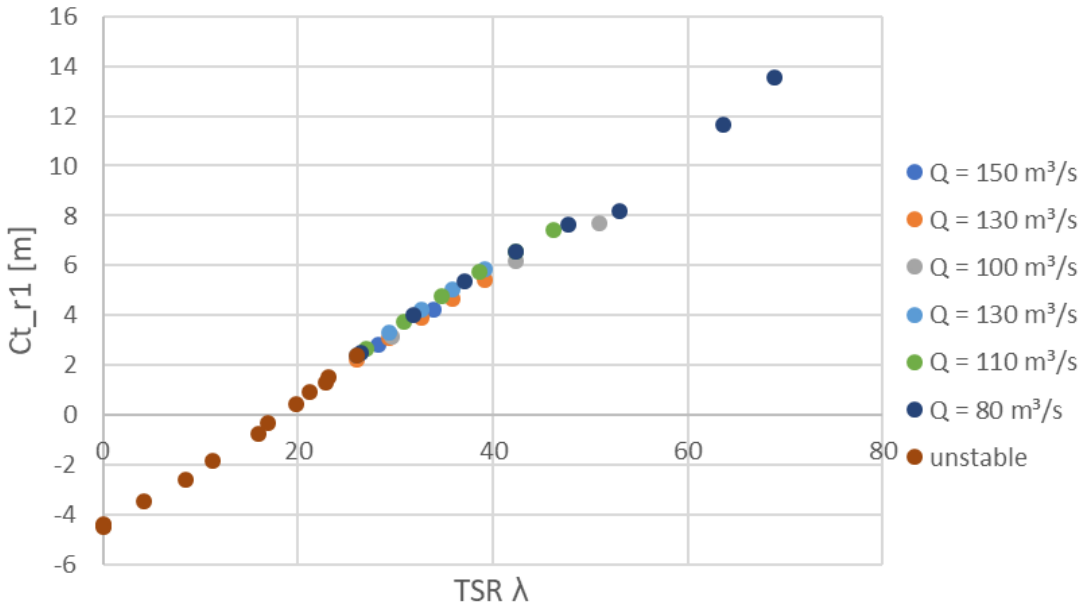

Figure 10: Ct_{r1} vs. TSR for different flow rates Q [m³/s]

3.2.3 Total pump head

Also for representation of h_{RPT}, the same variable is used as in turbine mode. Ch vs. TSR is plotted for different flow rates in Fig. 12. Ch is represented by a 3rd order polynomial curve with an R-square value of 0.9886 and RMSE of 0.1036.

$$Ch = \frac{h_{\mathrm{RPT}}}{Q^2} \tag{18}$$

$$Ch = 10^{-3} \cdot (1.987 \cdot 10^{-5}\ \lambda^3 - 0.003509\ \lambda^2 + 0.2375\ \lambda - 4.132) \tag{19}$$

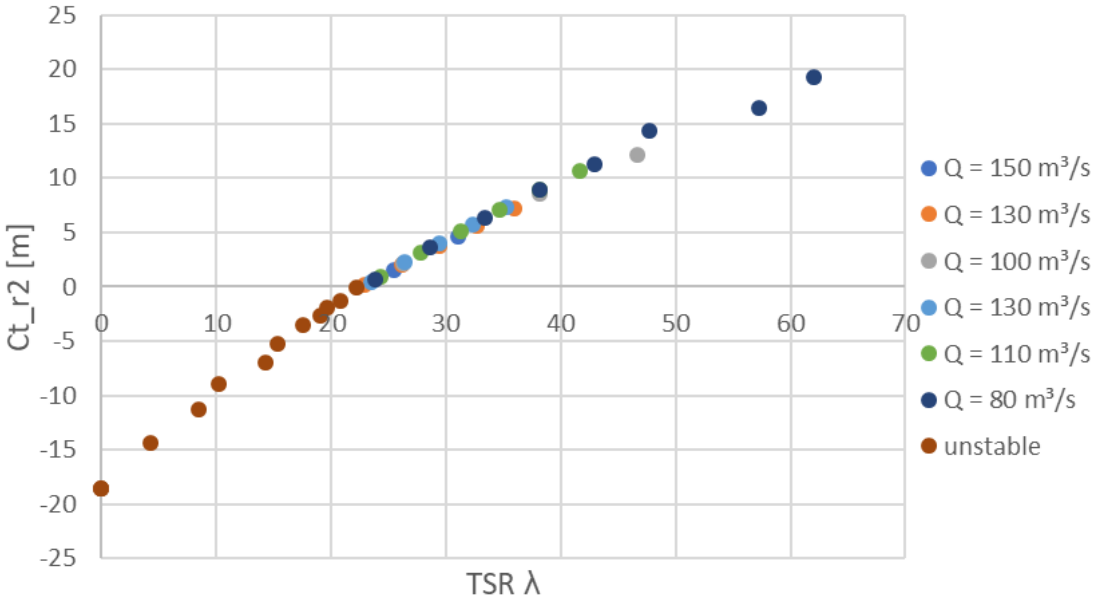

Figure 11: Ct_{r2} vs. TSR for different flow rates Q [$\mathrm{m^3/s}$]

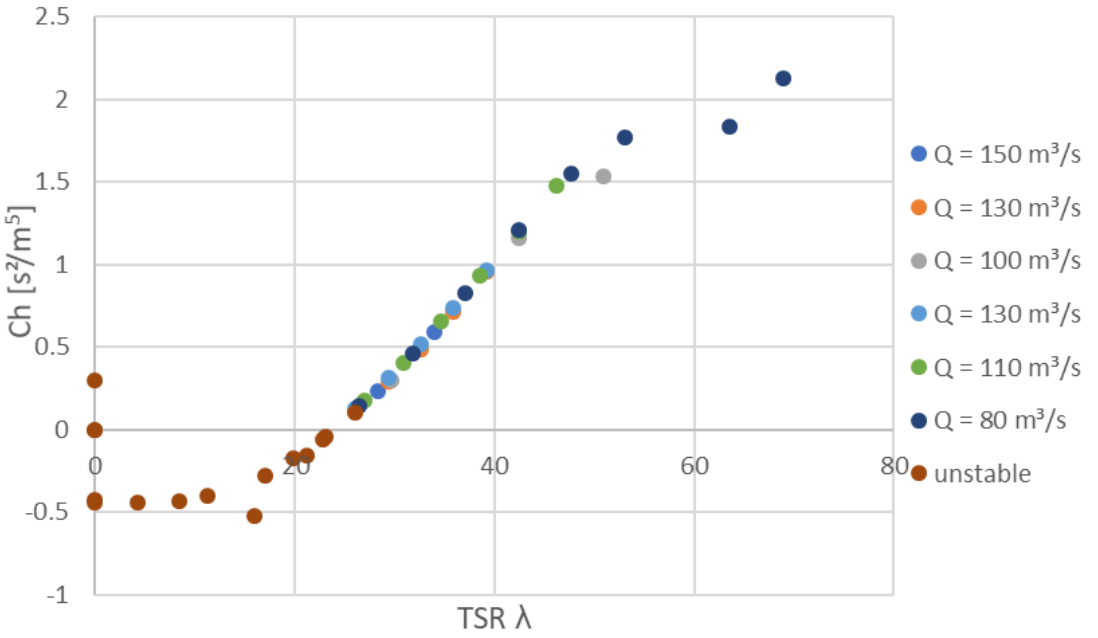

Figure 12: Ch vs. TSR for different flow rates Q [$\mathrm{m^3/s}$]

4 Static water flow model

The water flow model is used to define how the total RPT head h_{RPT}, inlet vane angle α and reservoir head difference Δh alters the flow rate Q. If Q is known, T_{R1} and T_{R2} can in turn be found from the curve fits given in section 3. Equation (20) shows the relation between Q, Δh and h_{RPT}, where Q is positive in turbine mode. This equation is derived from the energy conservation equation. The full derivation is elaborated in appendix A. Important to note is that the following assumptions were made:

- Steady and incompressible flow
- No reservoir pressure difference or head change
- Constant tube diameter
- Wholly turbulent flow

Therefore, the static water flow model presented here is an approximation, suitable for building up a simulation model, but to be refined at a later stage.

$$\mathrm{sgn}(Q) \cdot Q^2 = \frac{\pi^2 \ D^4 \ g \ (\Delta h - h_{\mathrm{RPT}}(Q))}{8 \ (k_c + k_v(\alpha))} \tag{20}$$

In (20), k_c represents the coefficient of constant major and minor losses and can be calculated or determined experimentally. In the initial simulations, $k_c = 4.5$. This value is an estimation for a system with a tube length of 800 m with two 90° elbows. $k_v(\alpha)$ is the coefficient of minor loss of the inlet vanes and depends on inlet vane angle α. In this deliverable, α can range from 0 (open) to 1 (closed). From the values in Fig. 13, we can fit a curve between the values for a gate valve. Additionally to the given operating points, we know that there is no flow when the gate is fully closed ($\alpha = 1$) and thus $k_v(1) = \infty$. The minor loss coefficient of the inlet vanes $k_v(\alpha)$ is plotted vs. α in Fig. 14.

$$k_v = \frac{-1348/75 \ \alpha^3 + 41/5 \ \alpha^2 - 128/75 \ \alpha}{\alpha - 1} \tag{21}$$

As seen in section 3, h_{RPT} is a function of Q and Ω_1. Therefore, h_{RPT} can be substituted into (20), resulting in an algebraic function of Q, Ω_1, Δh and $k_v(\alpha)$. If Q is known for a certain operating point, T_{r1} and T_{r2} can be calculated from regression curves for Ct_{r1} and Ct_{r2}.

Figure 13: Minor losses coefficients for valves in different opening states [2]

No	Type of valve	A coefficient of minor loss
1	Globe valve, fully open	10
2	Angle valve, fully open	2
3	Gate valve, fully open	0,15
4	Valve gate, ¼ closed	0,26
5	Gate valve, ½ closed	2,1
6	Gate valve, ¾ closed	17
7	Fully open ball valve	*0,05*
8	Gate valve, ⅓ closed	5,5

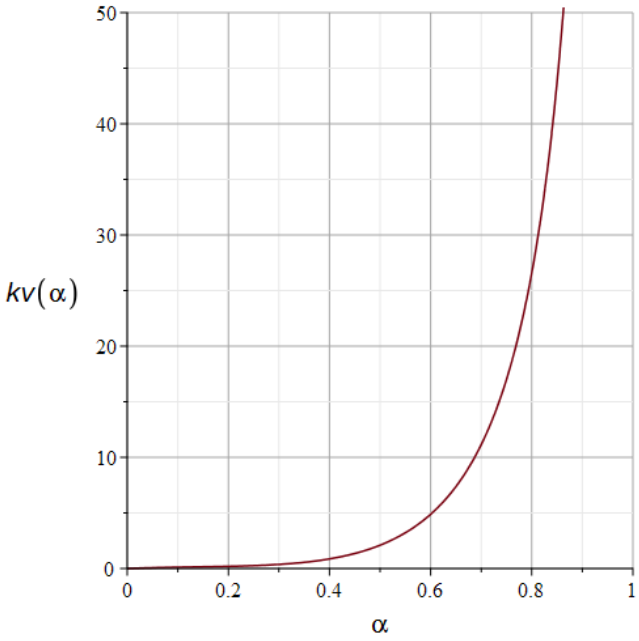

Figure 14: Minor loss coefficient of the inlet vanes $k_v(\alpha)$ vs. α

In the initial water flow model, the influence of the RPT's rotational speed, its head and the inlet vanes on the flow rate is discussed for turbine mode. Since modelling flow rate in pump mode depends on the stability of the pump in a certain operating range, this will be explained in section 6.2. h_{RPT} can be found through the regression curve for Ch_{RPT} vs. TSR. In turbine mode:

$$\begin{aligned} h_{\mathrm{RPT}} &= Q^2 \left(5.067 \cdot 10^{-7}\ \lambda^2 - 6.567 \cdot 10^{-5}\ \lambda + 0.001825\right) \\ &= 5.067 \cdot 10^{-7}\ (\Omega_1\ R\ A)^2 - 6.567 \cdot 10^{-5}\ (\Omega_1\ R\ A)\ Q + 0.001825\ Q^2 \end{aligned} \tag{22}$$

Implementing this equation into (20), a 2nd order function of Q is derived. From this equation, Q can be calculated if the rotational speed Ω_1, the position of the inlet vanes α (and thus minor loss coefficient $k_v(\alpha)$) and the head difference Δh

are known.

$$\left(\frac{\text{sgn}(Q)\ 8\ [k_c + k_v(\alpha)]}{\pi^2 D^4 g} + 0.001825\right)\ Q^2 + \tag{23}$$

$$(-6.567 \cdot 10^{-5}\ \Omega_1\ R\ A)\ Q + \tag{24}$$

$$[-\Delta h + 5.067 \cdot 10^{-7}\ (\Omega_1\ R\ A)^2] = 0 \tag{25}$$

If Δh is known, Q can be plotted vs. Ω_1 and $k_v(\alpha)$. Fig. 15 shows a contourplot with color indication of Q vs. Ω_1 and $k_v(\alpha)$ for $\Delta h = 14$ m. In the figure, the light blue curve represents the relation between $k_v(\alpha)$ and Ω_1, for which the TSR $\lambda = 32.5$. As discussed in section 3, the operating range is unstable for $\lambda > 32.5$. Stable operation is thus on the left side of the curve. Note that in stable operation, Q is proportional with Ω_1 and inversely proportional with $k_v(\alpha)$. Fig. 16 shows Q vs. Ω_1 for different values of $k_v(\alpha)$, where $\Delta h = 14m$. Fig. 17 shows Q vs. Ω_1 for different values of Δh, where $k_v(\alpha) = 0$.

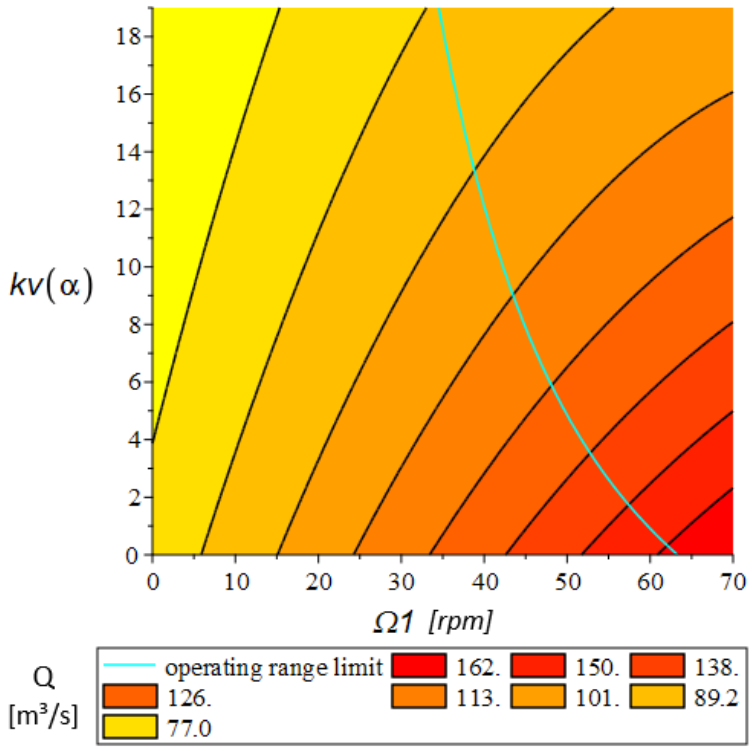

Figure 15: Contourplot with color indication of Q [m³/s] versus Ω_1 [rpm] and $k_v(\alpha)$ for $\Delta h = 14m$

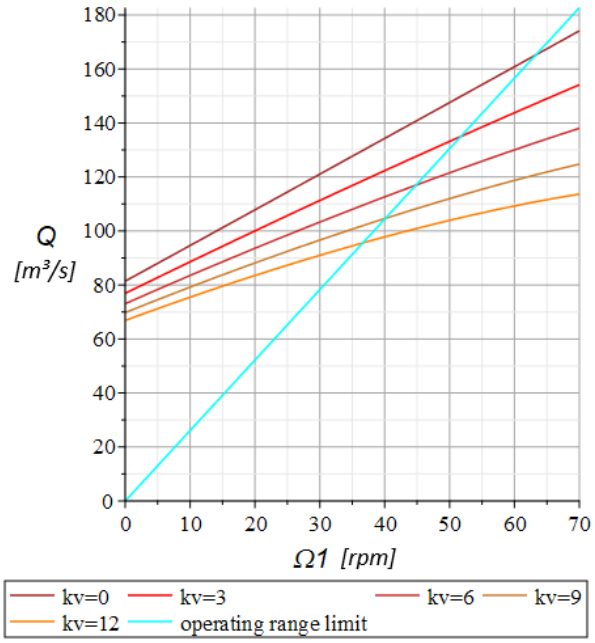

Figure 16: Q [m^3/s] vs. Ω_1 [rpm] for different values of $k_v(\alpha)$, where $\Delta h = 14m$

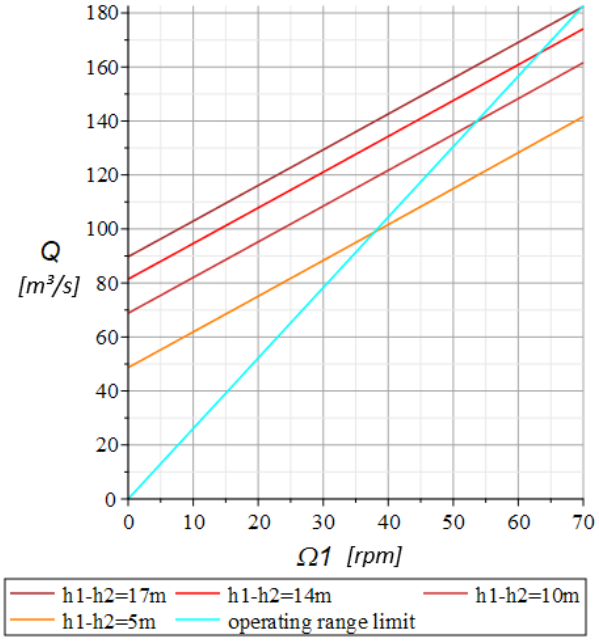

Figure 17: Q [m^3/s] vs. Ω_1 [rpm] for different values of Δh, where $k_v(\alpha) = 0$

5 Low level control

The aim of the low level control is to realise the torque setpoints determined by the high level control, for each PMSM, by regulating the currents injected to the three-phase stator windings of the PMSM. The low-head pumped hydro concept developed in ALPHEUS requires fast control of power, and thus torque, to offer flexibility to the grid. Therefore, the use of Field Oriented Control (FOC) as a special case of vector control is envisioned to regulate the PMSM torque. The general concept behind both field orientation and vector control is to regulate the currents i_d and i_q as constant values in the rotating reference frame. i_d and i_q are related to phase currents i_a, i_b and i_c through the Clarke-Park transform. A full explanation of the rotating reference frame and vector control is added in appendix B. Field orientation is a special case of vector control, where the d axis current setpoint $\hat{i}_d$ is set to zero. By doing so, the current vector i is aligned with the q axis of the rotor. No current flows in the d axis scheme and the armature reaction voltage $\Omega_e L_d i_d$ in the q axis becomes zero. Therefore, also the reluctance torque becomes zero and the torque equation simplifies to:

$$T = N_p \frac{3}{2} \Psi_{\mathrm{PM}} i_q \tag{26}$$

Here, N_p is the pole pair number and Ψ_{PM} is the constant flux of the permanent magnets. The torque is directly proportional to one single control variable, i.e., the q axis current i_q. When giving a torque setpoint to a PMSM drive in field oriented mode, this setpoint is internally simply treated as an i_q setpoint with a proper scaling factor as given by the above equation. The concept of regulating torque with a single current value makes field orientation the most popular control technique for PMSM drives, as it results in desirable control dynamics.

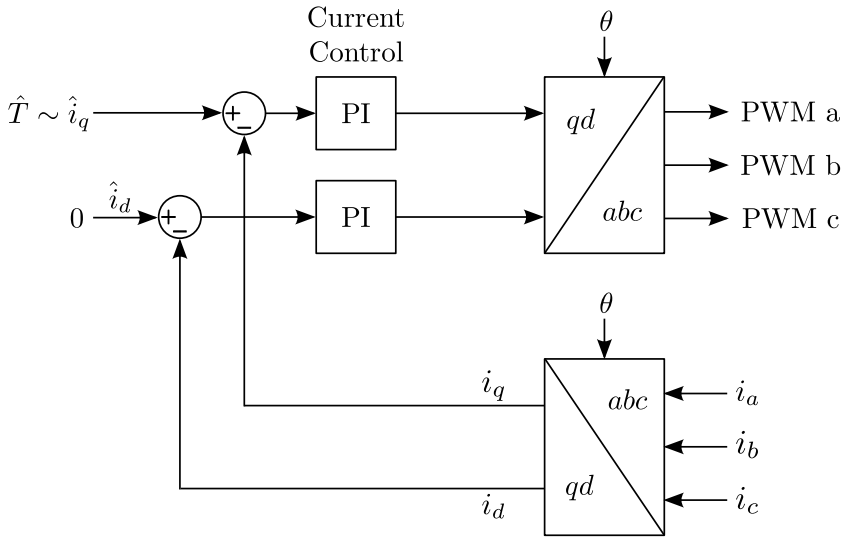

Figure 18: Implementation of field orientation for a PMSM

As already mentioned, in some cases the low level control also includes the realisation of the rotational speed Ω. The high level control then outputs two speed setpoints, instead of torque setpoints. One possibility is to use cascaded control, as shown in Fig. 19. Here, the difference between the speed setpoint and actual measured speed corresponds to a torque setpoint, which is handled by the field oriented control. To achieve a more dynamic model, a feed-forward can be used. This feed-forward can e.g. be the expected back-EMF, calculated based on the rotor speed.

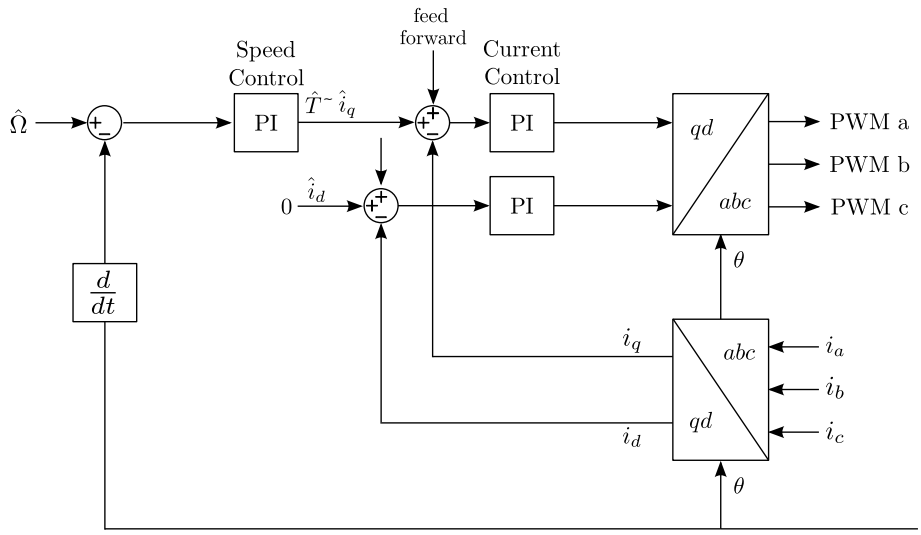

Figure 19: Cascaded speed control for a PMSM

6 High level control

The goal of the high level control is to realise a power setpoint $\hat{P}$ with dynamics and efficiency in mind, while maintaining the system's stability. Additional boundary conditions can be taken into account by the high level control as well, such as limitations on the mechanical stresses and loads to avoid fatigue. Another possibility is to reach a certain operating point with a minimal or maximal flow rate Q. This is valuable in a system with limited reservoir capacity. Although valid system sites are still being investigated, the benefit of this extra constraint can be explained through an example. In the example site, the lower reservoir capacity is quasi infinite (e.g. the sea) and the upper reservoir capacity is limited. Here, the upper reservoir gets drained in turbine mode and filled in pump mode. Since both turbine and pump efficiency $< 100\%$, the upper reservoir would experience a relative decrease in water level, when turbining and pumping for the same amount of time at the same power setpoint. Furthermore, grid data shows that underfrequency is more common than overfrequency. Therefore, the system will be used more in turbining mode. These results show that the system would most likely benefit from a control algorithm, that works at the lowest possible flow rate in turbine mode and at the highest possible flow rate for pump mode. However, situations may exist where the opposite is necessary. E.g. when the system is pumping for a large amount of time, the upper reservoir water level can get too high. Here, the control algorithm can then switch to working at the lowest possible flow rate in pump mode. However, this chapter will focus mostly on the first.

Note that in this section, high level control concepts are described that use the predefined speed ratio of $\zeta = \frac{\Omega_1}{\Omega_2} = 0.9$. Therefore, the influence of control parameters Ω_1 and $k_v(\alpha)$ is discussed. Here, Ω_2 is controlled such that it always operates at a ratio of 90% of Ω_1. Such a master-slave control system is something that will also be used for the positive displacement RPT, discussed in section 8, where the relative position between the runners is of great importance. Control concepts with variable speed ratio are further discussed in section 7.

6.1 Turbine

Since total power can be calculated for a known Ω_1 and Q (see section 3), this means that if Δh remains constant, each couple of Ω_1 and $k_v(\alpha)$ corresponds with a power point. This can also be seen in the contourplot in Fig. 20. It can be seen that the power experiences a maximum for a certain rotational speed Ω_1, after which the power decreases with speed. Furthermore, the power decreases with an increase of the minor losses, caused by the inlet vanes $k_v(\alpha)$. The limit of operating range is again indicated with a light blue color.

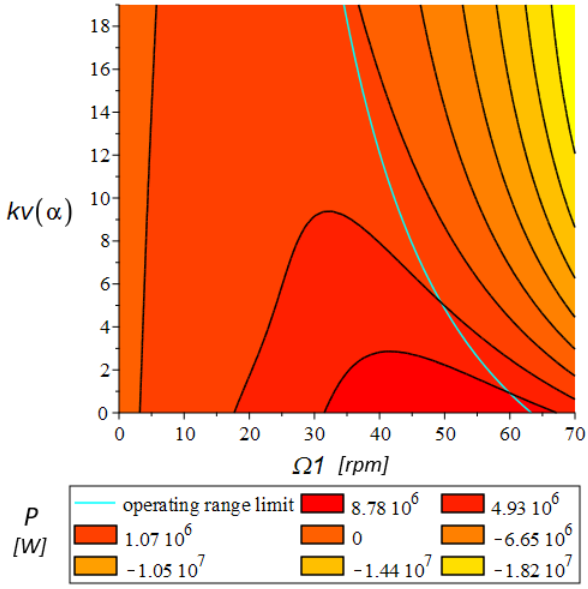

Figure 20: Contourplot with color indication of power P [W] vs. Ω_1 [rpm] and $k_v(\alpha)$

Fig. 21a shows P vs. Ω_1 for different values of $k_v(\alpha)$, where $\Delta h = 14$ m. Here it can be seen that small changes in $k_v(\alpha)$ have a great effect on power and the rotational speed at which power is maximal. Fig. 21b shows P vs. Ω_1 for different values of Δh, where $k_v(\alpha) = 0$. Note that the power P is highly dependent on the head difference. Furthermore, at lower head, the maximum power is reached at a lower rotational speed Ω_1.

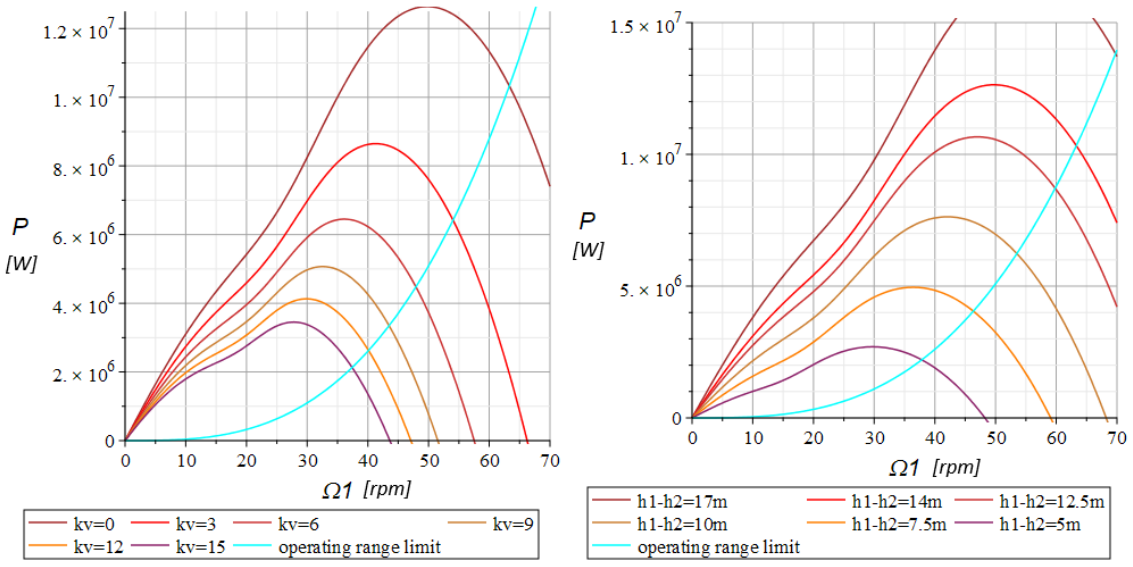

(a) (b)

Figure 21: P [W] vs. Ω_1 [rpm] for different values of (a) $k_v(\alpha)$ and (b) Δh, where $k_v(\alpha) = 0$

6.1.1 Robust P&O algorithm with one variable control parameter

If the system is not perfectly known (such as the value of major and minor losses k_c or the exact values of $k_v(\alpha)$ in function of control parameter α), it is hard to predict the influence of Ω_1 and $k_v(\alpha)$ on the flow rate Q and thus output power P. Therefore, a robust Hill-Climb (Perturb & Observe (P&O)) control algorithm can be used in this case. Here, small increments or perturbations are inflicted to the rotor speed Ω_1. If the new power after these changes is closer to the power setpoint, the algorithm continues in this direction. If the new power is further from the power setpoint, it reverses the direction of Ω_1. This control is thus based on one control parameter Ω_1, which is altered to reach the power setpoint $\hat{P}$. $k_v(\alpha)$ is in this control system used for startup and stop methods, as well as safety functions.

Fig. 22 shows a basic P&O algorithm. Here, k is the step size. Based on if the current power is closer or further to power setpoint $\hat{P}$ than the previous power, r respectively preserves and reverses the direction of $\Delta\Omega_1$. E.g. if the Ω_1 is incremented, and the actual power is closer to $\hat{P}$, Ω_1 is again incremented. The power can be calculated from Q or directly measured from the machine power. If it is calculated from Q, then Q needs to be calculated or measured.

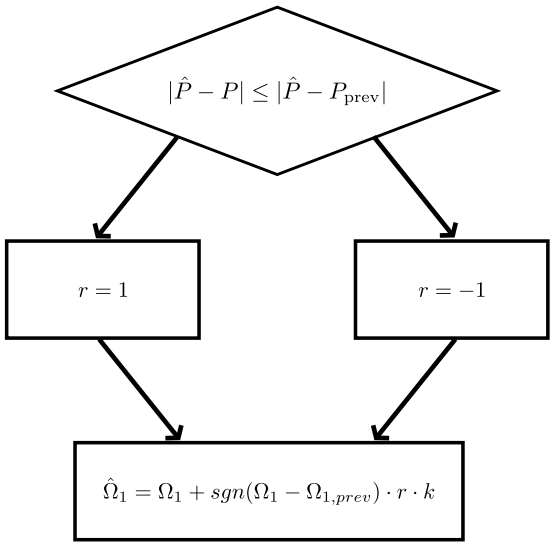

Figure 22: Basic P&O algorithm flowchart

Fig. 23 shows an improved algorithm, where step size k is adaptive. If the rotational speed is moving in the right direction (and $r == r_{prev}$), k is incremented to reach $\hat{P}$ faster. If $\hat{P}$ is reached, power P fluctuates around setpoint $\hat{P}$, because it constantly increments or decrements Ω_1. To limit the fluctuations, k is decremented when Ω_1 has to change directions and thus $r <> r_{prev}$. The first time the rotational speed changes direction, k can be large. Therefore, if rotational speed changes direction and $k >$ initial step size k_0, it is reset to that step size.

Next, if the system has been fluctuating among a certain $\hat{P}$, $k < k_0$ and the step size is small. Therefore, if the power setpoint changes, k is also reset to k_0 to ensure optimal response to the new power setpoint.

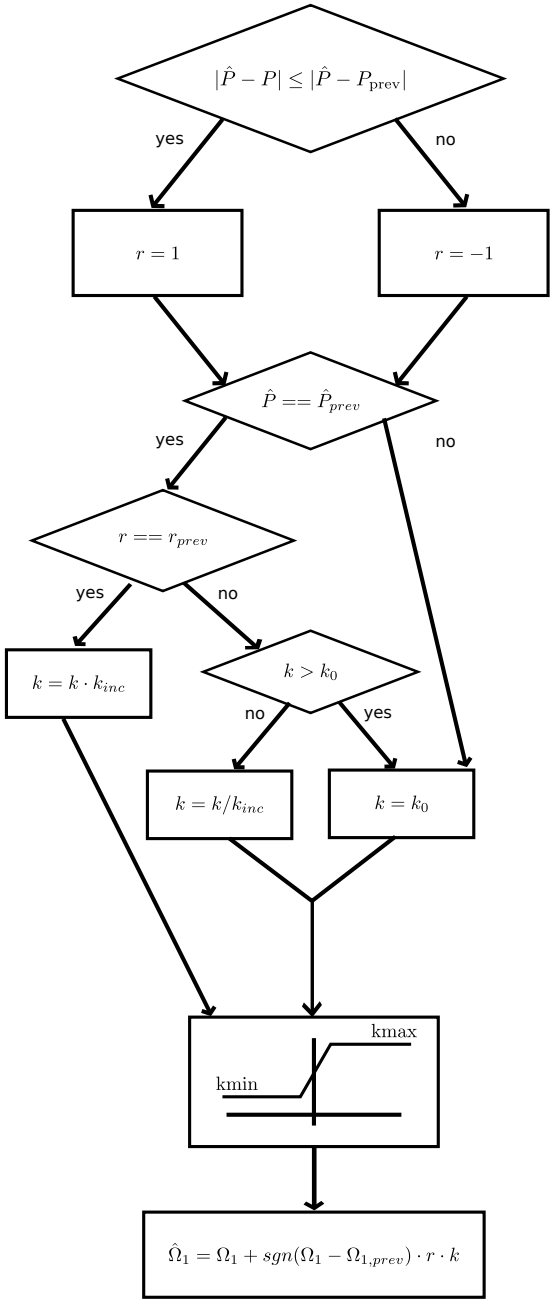

Figure 23: Adaptive P&O algorithm flowchart

As can be seen from Fig. 21a, the curves can be split into the left side, where $dP/d(\Omega_1) > 0$ and the right side, where $dP/d(\Omega_1) < 0$. For a combination of Δh and $k_v(\alpha)$, a power setpoint $\hat{P}$ corresponds with two possible rotational speeds

Ω_1. Therefore, the described algorithm will automatically go to one of these possible points, depending on its previous state. However, only one of these points is optimal. The point with the smallest rotational speed Ω_1 works at the lowest flow rate Q, as can be seen in Fig. 17. Furthermore, if the system is at the right side of the curve, it is at risk of ending up outside the operating range. Therefore, the control system is more efficient and robust if it only operates at the right side of the curve, where $dP/d(\Omega_1) > 0$. This can be done by verifying if $\text{sgn}(dP)\text{sgn}(d(\Omega_1)) > 0$ every iteration. If this is not the case, Ω_1 has to be decremented until the above case is true. This single variable control system is robust, since it doesn't require excellent knowledge about the system. Therefore, its precision and dynamics keep constant through changing environmental elements. However, it does not reach the optimal efficiency point, as will be discussed in the following subsection. Furthermore, a P&O algorithm is a relatively slow algorithm, because of its reactive nature with trial-and-error method.

6.1.2 Control algorithm with two variable control parameters

As visualised in Fig. 20, P can be described as a function of Ω_1 and $k_v(\alpha)$. Therefore, each power setpoint $\hat{P}$ corresponds with an implicit relation between Ω_1 and $k_v(\alpha)$:

$$P(\Omega_1, k_v(\alpha)) = \hat{P} \tag{27}$$

Fig. 24 illustrates this implicit relation for different power setpoints at $\Delta h = 14m$. Hence, for every power setpoint $\hat{P}$, an infinite amount of combinations for Ω_1 and $k_v(\alpha)$ exists. Therefore, the control system could go to the point that is closest to its current operating state. However, it is also possible to impose another constraint, such as lowest flow rate Q. Doing this, the turbine is ensured to work at the lowest possible flow rate, and thus draining upper and filling lower reservoir slower. In Fig. 25, the implicit curves for Ω_1 and $k_v(\alpha)$ are projected on the three-dimensional contourplot for Q vs. Ω_1 and $k_v(\alpha)$, which is also seen in Fig. 15. On this representation, it can be seen that the lowest flow rate is not always reached at $k_v(\alpha) = 0$ and minimal Ω_1, which is how power setpoints are reached with the single variable P&0 control system, described in the previous section. The lower the power setpoint, the more the lowest Q point differs from the operating point at $k_v(\alpha) = 0$. Therefore, controlling Ω_1 and $k_v(\alpha)$ simultaneously, can have a significant advantage. Since large order functions cannot be solved in real time, a lookup table is used. In this lookup table, the combination of Ω_1 and $k_v(\alpha)$ is stored for multiple head differences Δh and multiple power setpoints $\hat{P}$. In system operation, the appropriate point is then selected by choosing the stored operating point that is closest to the current head difference and power setpoint or by using linear interpolation between two stored operating points in the lookup table. If the desired $\hat{\Omega}_1$ and $k_v(\alpha)$ are reached, a P&O algorithm is further used to reach the desired power setpoint exactly. This is necessary, because:

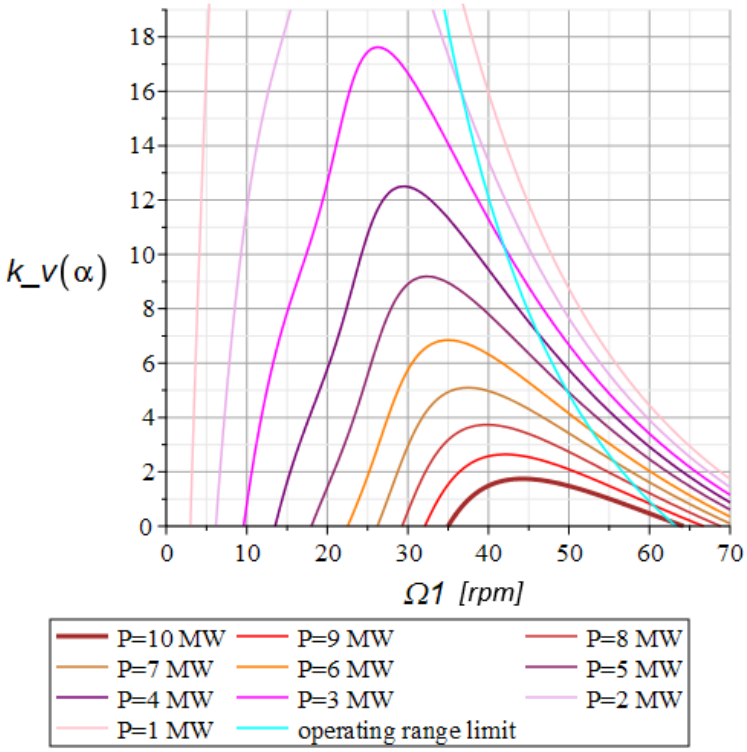

Figure 24: Relation between $k_v(\alpha)$ and Ω_1 [rpm] for different power setpoints $\hat{P}$, at $\Delta h = 14m$

- the stored points are calculated based on exact values for Δh, which have an error upon measurement
- the stored points are calculated based on a constant k_c that describes the tubing system major and minor losses, which can change in time
- the interpolation introduces a small error due to the linear approximation

Note that it is also possible for multiple lookup tables to be stored, for different constraints. E.g. a lookup table can be constructed to find Ω_1 and $k_v(\alpha)$ for the highest possible flow rate Q. The high level control can then switch between both lookup tables, depending on reservoir head state.

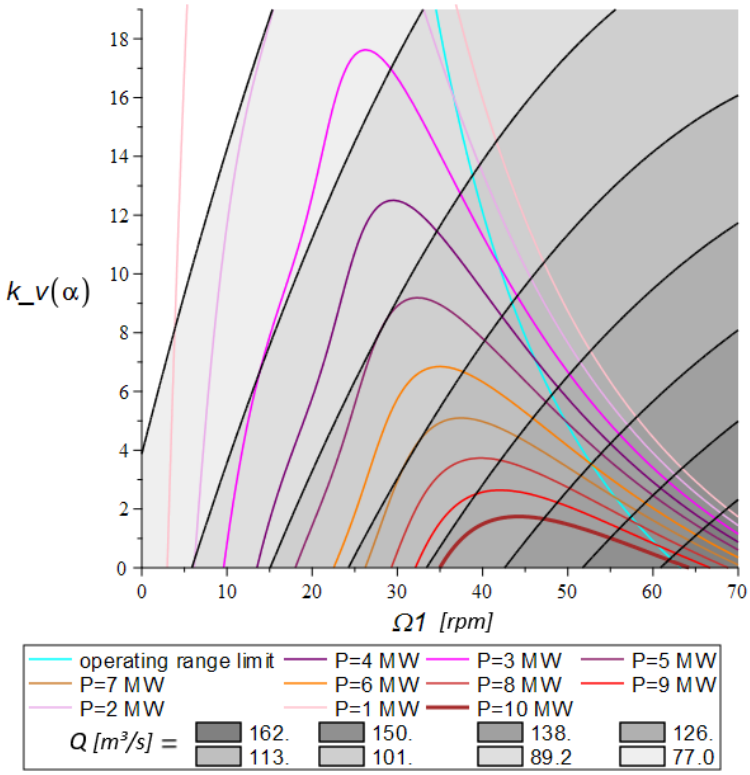

Figure 25: Relation between $k_v(\alpha)$ and Ω_1 [rpm] for different power setpoints $\hat{P}$, projected on 3D plot of $Q(\Omega_1, k_v(\alpha))$ [$\mathrm{m^3/s}$] for $\Delta h = 14$ m

6.1.3 Startup and stop method

As seen in section 3, T_{r1} and T_{r2} are inversely proportional to rotational speed. At $\Omega = 0$, both T_{r1} and T_{r2} are maximal. Fig. 26 shows two contourplots for T_{r1} and T_{r2} vs. Ω_1 and $k_v(\alpha)$. In this contourplot, the inverse relation can be observed. Furthermore, for a given rotational speed, increasing $k_v(\alpha)$ reduces flow rate Q and thus also T_{r1} and T_{r2}. However, starting torque is always > 0 for every possible $k_v(\alpha)$. As seen in section 4, the minor loss coefficient of the runner vanes $k_v(\alpha)$ is a function of α, which can reach from $0\% - 100\%$. Fig. 27 shows how the starting torque for both runners changes over the range of α. It can be concluded that the turbine is completely self-starting. Therefore, the startup method in turbine mode consists of opening the inlet valves with $k_v(\alpha)$. Doing this will automatically increase runner speeds Ω_1 and Ω_2, which can then be controlled to reach the power setpoint $\hat{P}$ based on the chosen control strategy.

Next, the stop method will be discussed. When stopping, a braking torque is imposed on the runners. Therefore, the inlet vanes should be closed, while simultaneously slowing down turbine speeds Ω_1 and Ω_2. Doing this simultaneously

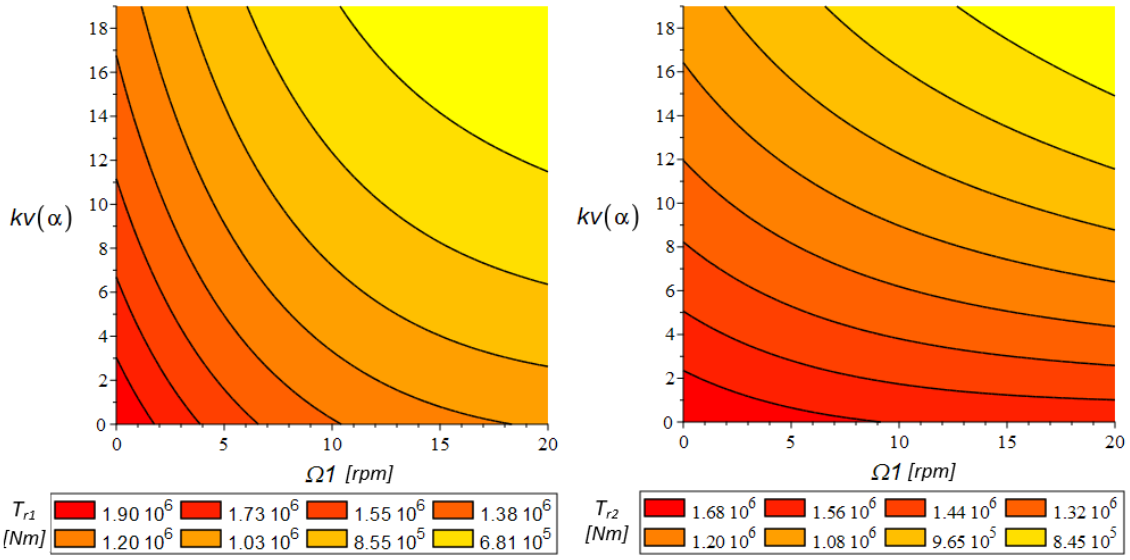

(a) (b)

Figure 26: Contourplot of (a) T_{r1} [Nm] and (b) T_{r2} [Nm] vs. Ω_1 [rpm] and $k_v(\alpha)$ at low rotational speeds for $\Delta h = 14$ m

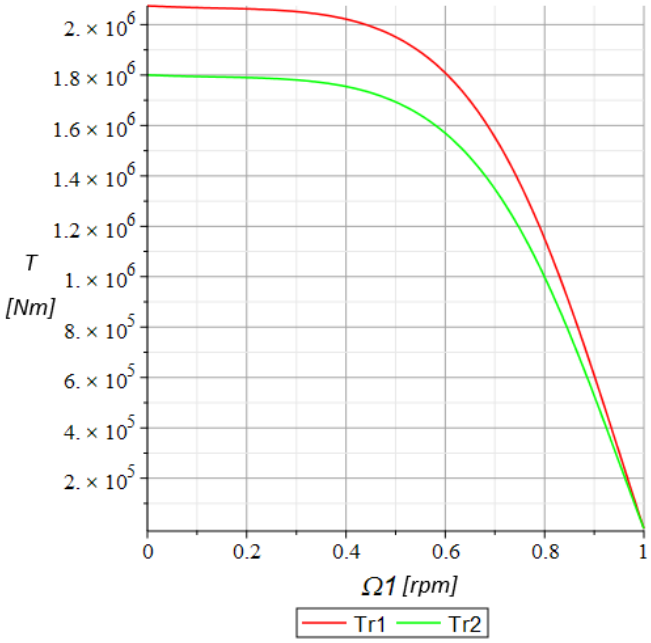

Figure 27: Starting torque (a) $T_{r1,0}$ [Nm] and (b) $T_{r2,0}$ [Nm] vs. α for $\Omega = 0$ rpm and $\Delta h = 14$ m

avoids the large peak torque the low level control experiences, since the starting torque T_0 also decreases with increasing α and thus $k_v(\alpha)$. Furthermore, when $\alpha = 0$, the flow rate $Q = 0$ and thus no water flow 'waste' is present.

6.2 Pump

Initially, control in pump mode is analysed for a single control variable, which is the rotational speed Ω_1, with a constant speed ratio and thus $\Omega_2 = 0.9\ \Omega_1$. Therefore, $\alpha = 0$ and thus $k_v(\alpha) = 0$. The influence of the inlet vanes will later be elaborated on in subsection 6.2.5.

6.2.1 Stability

In pump-mode, the system is more susceptible for instability. First, the pump cannot operate under or over its minimal and maximal tip speed ratio respectively. Otherwise, cavitation and high internal torques may arise, which are deleterious for the pump. Furthermore, the pump has to generate enough head to overcome Δh, as well as the major and minor losses. Equation 28 shows the relation between h_{RPT}, Q and Ω_1. Fig. 28a visualises this relation for a rotational speed of $\Omega_1 = 50$ rpm. It can be seen that for a set h_{RPT}, multiple possible flow rates exist. It should be noted that there were only few CFD calculations for the low flow rates (below minimum Q), since this is beyond the maximum TSR. Therefore, the curve shape here can differ.

$$h_{\mathrm{RPT}} = 10^{-3} Q^2 \left[1.987 \cdot 10^{-5} \left(\frac{\Omega_1\ R\ A}{Q} \right)^3 - 0.003509 \left(\frac{\Omega_1\ R\ A}{Q} \right)^2 + 0.2375 \frac{\Omega_1\ R\ A}{Q} - 4.132 \right] \tag{28}$$

Fig. 28b shows the relation between h_{RPT} and Q for a number of rotational speeds. The operating range limits (minimal and maximal TSR) are indicated by light blue pointplots. Note that for lower rotational speeds, h_{RPT} decreases, as well as the flow rate range for which operation is stable.

In section 4, it was discussed that the flow rate Q can be found from equation (20). Reshaping this equation gives:

$$h_{\mathrm{RPT}}(Q) = \Delta h + h_L(Q) \tag{29}$$

where $h_L(Q)$ is given by the equation below and thus proportional to Q^2. In early simulations $k_c = 4.5$. Fig. 29 shows what is commonly called the system curve, which is the relation between $\Delta h + h_L$ and flow rate Q, for $\Delta h = 7$ m and $k_v(\alpha) = 0$. This visualises how h_L increases with Q.

$$h_L(Q) = [k_c + k_v(\alpha)] \frac{8}{\pi^2\ D^4} \frac{Q^2}{g} \tag{30}$$

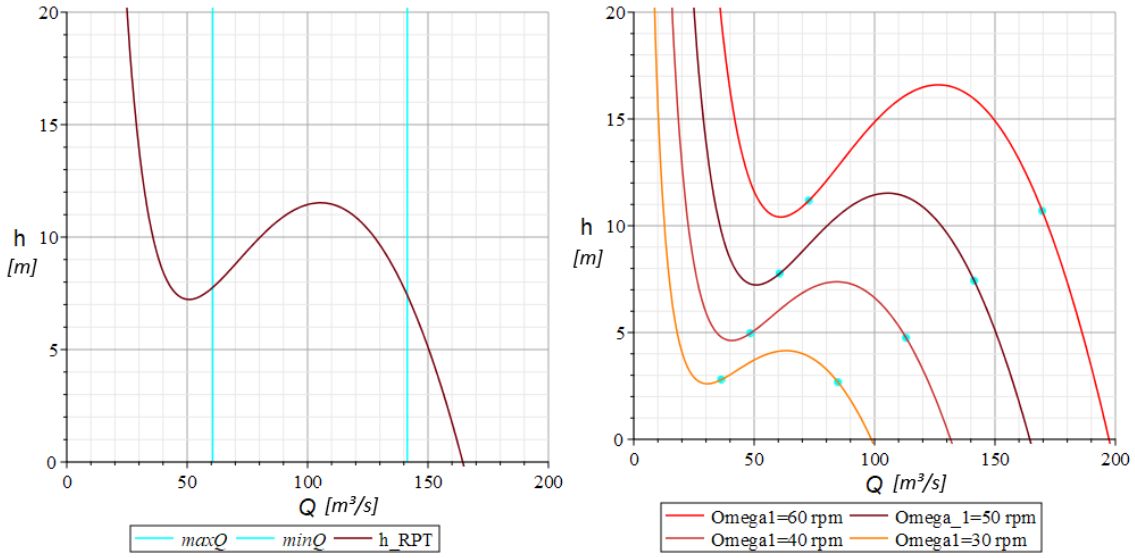

(a) (b)

Figure 28: h_{RPT} [m] vs. Q [m^3/s] (a) for a set rotational speed of $\Omega_1 = 50$ rpm (b) for different rotational speeds Ω_1 [rpm]

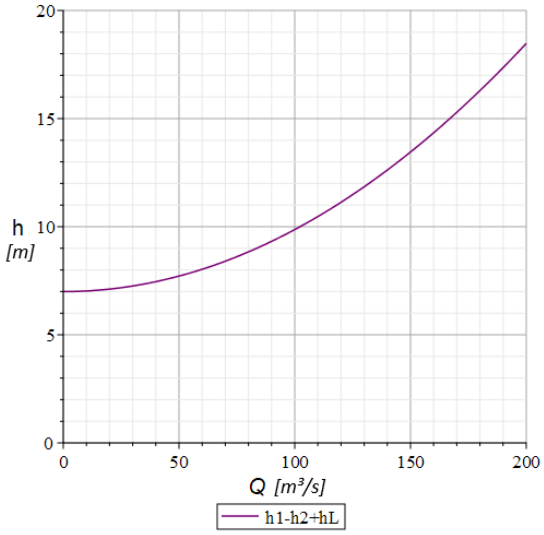

Figure 29: System curve for $\Delta h = 7$ m and $\mathrm{k}_v(\alpha) = 0$

The operating point and thus system flow rate Q can be found by finding where the pump curve $h_{\mathrm{RPT}}(Q)$ intersects with the system curve $\Delta h + h_L(Q)$. To discuss the stability of the pump for different head heights, Fig. 30 illustrates the pump curve for $\Omega_1 = 50$ and the system curves for different head heights Δh, with $k_v(\alpha) = 0$. Here the different scenarios of head heights are discussed:

- If Δh is 10 m, there is one intersection between pump and system curve. However, since this operating point is below the minimal flow rate Q (and thus above maximal TSR λ), this point is outside the operating range. Therefore, it is unsure if the pump is stable in this region. Since the flow rates in this region are considerably lower than the design flow rate, for now it is presumed that the pump is unstable. However, further research at these low flow rates could prove otherwise [4].

- If Δh is 7 m, there are multiple intersections. This means that the pump can operate at different flow rates. This is not a stable operating mode, since the flow rate can fluctuate between the different operating points [4]. Therefore, the system is unstable in this region.

- If the head height is 3 m, there is one intersection between pump and system curve. Therefore, the system will experience stable operation at the flow rate at intersecting point of $Q = 135\text{m}^3/\text{s}$, for a given head height and rotational speed.

- If Δh is too low (towards 0 m), it might occur that the intersection (and thus operating point) is on the right side of the maximal Q (and thus minimal TSR). In this case, the system is also unstable. Especially for lower rotational speeds, this needs to be taken into account.

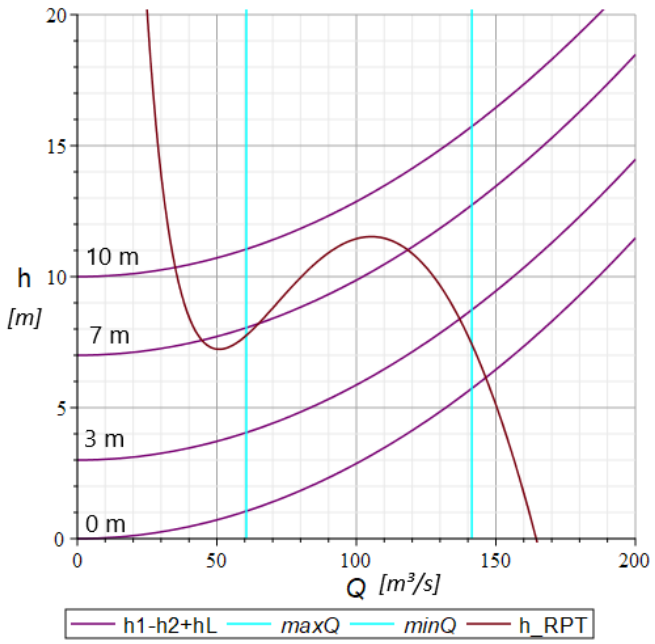

Figure 30: Pump curve and system curves for different head heights Δh [m], and $\Omega_1 = 50$ rpm

6.2.2 Modelling flow rate

The intersections between pump and system curves described above can be found by the following equation, which was discussed in section 4:

$$\frac{\mathrm{sgn}(Q)\ 8\ (k_c + k_v(\alpha))}{\pi^2\ D^4\ g} \cdot Q^2 - \Delta h + h_{\mathrm{RPT}}(Q, \Omega_1) = 0 \tag{31}$$

Therefore, at any moment if Δh, $k_v(\alpha)$ and Ω_1 are known, then Q can be determined. Fig. 31 shows how Q changes with rotational speed Ω_1 for different head heights and $k_v(\alpha) = 0$. Note that operation is only stable if the TSR λ is between minimal and maximal TSR, and there is only one solution for Q. Otherwise, the flow rate will fluctuate between the two operating points and will not be stable. It can be seen that for stable operation, at head height of 7 m, Ω_1 must be > 53 rpm, for 10 m, this becomes 63 rpm. Finally, for 3 m, $\Omega_1 > 35$ rpm. Note that for the curve for $\Delta h = 7m$, $\Omega_1 = 50$ gives the same 3 flow rates Q as in Fig. 30.

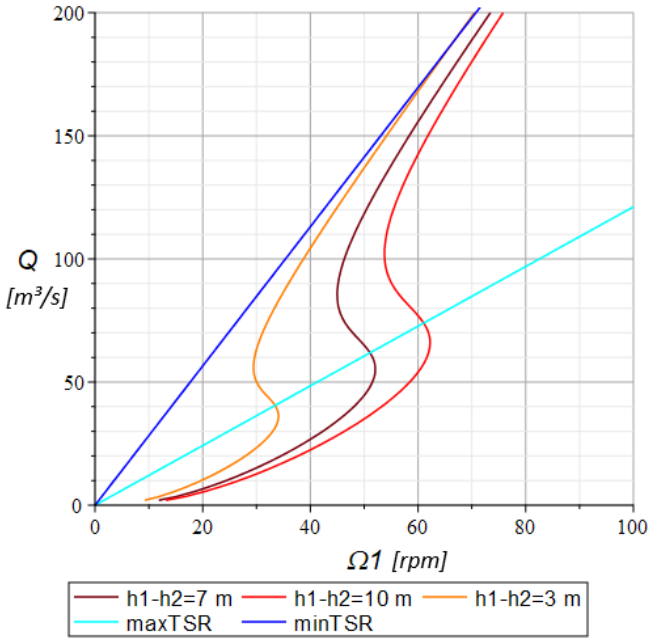

Figure 31: Flow rate Q [m³/s] vs. Ω_1 [rpm] for different head heights and $k_v(\alpha) = 0$

6.2.3 Power

Now that the lowest rotational speed Ω_1 for which the system is stable for a given head height Δh is known and the relation between Q and Ω_1 is known, the power needs to be calculated. When needed power P vs. Ω_1 for a given head height is known, Ω_1 can be chosen by the high level control to reach a given power setpoint $\hat{P}$. Fig. 32 shows power P vs. Ω_1 for the stable rotational speeds. An important difference with turbine mode, is that at a given head height, the power can only be reached by one rotational speed Ω_1. Note that, with the given flow modelling constant k_c given in section 4, at a head height of 10 m, a pump of 10 MW cannot operate stably. For $\Delta h = 7$ m, 10 MW is the minimal possible power setpoint $\hat{P}$. However, for a head height of 3 m, all power setpoints between 3 MW − 10 MW are possible.

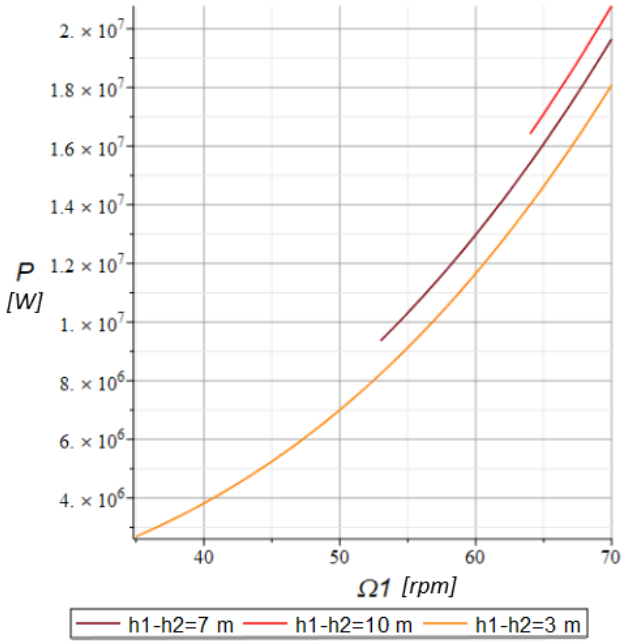

Figure 32: Power P [W] vs. rotational speed Ω_1 [rpm] for different head heights

6.2.4 Control system

The control system will again exist of a lookup table. In this lookup table, multiple values of P will be calculated for a number of head heights Δh and a number of rotational speeds Ω_1, where the system is stable. Between the stored points, linear interpolation can be executed in real time to find the optimal Ω_1. If the desired speed $\hat{\Omega}_1$ is reached, a P&O algorithm is further used to reach the desired power setpoint exactly. This is necessary because of inaccuracies in

system curve calculation and the linear interpolation. This P&O control system is similar to the one described in section 6.1.

Also, the limits of the system will be stored. Therefore, if a power setpoint is received that cannot be reached at the current head height, the control system will automatically go to the power setpoint that can be stably reached and is closest to the given power setpoint. For example, if $\Delta h = 7$ m and the power setpoint $\hat{P} = 9$MW, the control system will go to the lowest stable rotational speed, which in this case gives (or needs) a power of $P = 9.64$ MW.

6.2.5 Influence of inlet vane control

From the graphs shown in the previous subsection, it can be read that for the same power, Q is lower for a higher head difference. Since increasing $k_v(\alpha)$ can be seen as virtually increasing the net head difference, increasing $k_v(\alpha)$ will result in a lower flow rate Q. However, it is most likely that the RPT is required to operate at a maximal flow rate Q for a given power setpoint, for the same reasons as listed in the intro of section 6. However, for situations where it is necessary, the inlet vanes can be used to instead reach the operating point with lowest flow rate Q.

Fig. 33 shows the flow rate Q and power P vs. Ω_1 for different values of $k_v(\alpha)$. Note that for $k_v(\alpha) > 20$, the operating points correspond with a TSR which is lower than the minimal TSR. To explain the influence of the inlet vanes, an example is used for $\Delta h = 3$ m and a power setpoint of $\hat{P} = 8$ MW. Table 1 shows the values of Ω_1 and Q, that correspond with the power setpoint, for the different values of $k_v(\alpha)$. It is clear that increasing the inlet vane angle can reduce the operational flow rate Q, for the same power setpoint. However, for $k_v(\alpha) > 15$, the power setpoint is out of the operating range of the pump. To include control with minimal flow rate, another lookup table needs to be created that stores every combination of $k_v(\alpha)$ and Ω_1 for a given power setpoint $\hat{P}$ and head height Δh, similarly to what is done in turbine mode.

Table 1: Q and Ω_1 for $\Delta h = 3$ m and $\hat{P} = 8$ MW

$k_v(\alpha)$	Ω_1 [rpm]	Q [m^3/s]
0	52.5	145
5	50	117
10	50	95
15	52	71
20	unstable	unstable

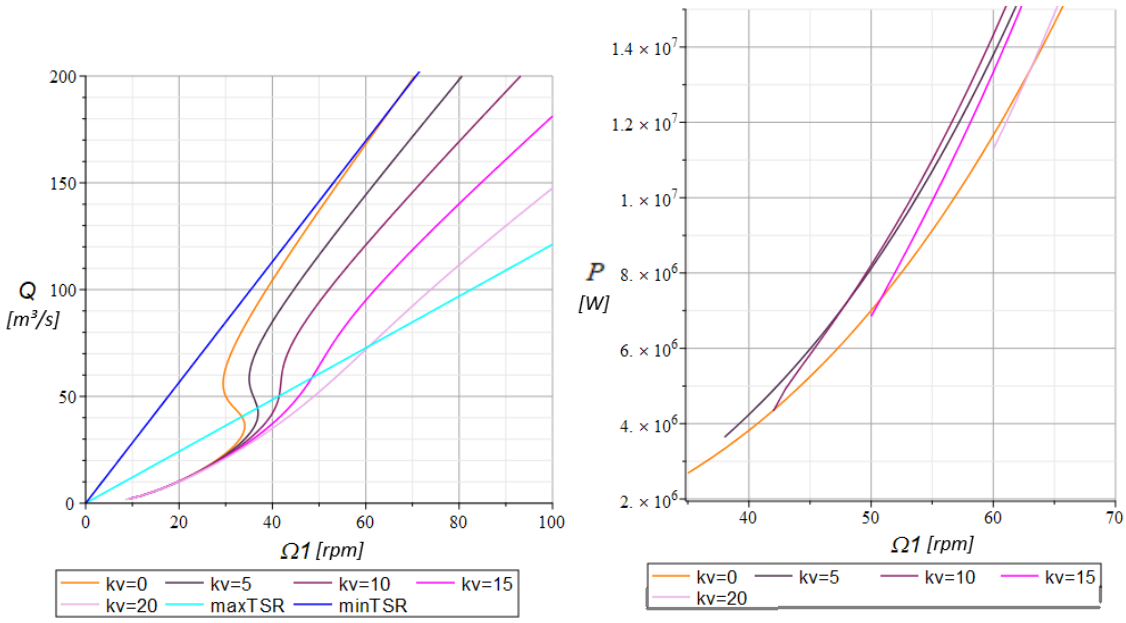

(a) (b)

Figure 33: (a) Q [m^3/s] and (b) P [W] vs. Ω_1 [rpm] for $\Delta h = 3$ m for different values of $k_v(\alpha)$

6.2.6 Startup method

The pump can only operate if a positive net head is reached. If this is not the case, the water would flow in the opposite direction. The pump cannot naturally reverse the natural flow direction, since this induces great internal torques. Therefore, startup in pump-mode consists of accelerating the runner speeds Ω_1 and Ω_2 up to a speed which corresponds with a total head $h_{\mathrm{RPT}} > \Delta h$, while the inlet vanes stay closed (α=1). Once the desired speed is reached, the inlet vanes open as fast as possible. Since this opening speed is limited by available torque of the inlet vanes, inertia etc., the loss of the inlet vanes $h_{L,v}$ is considerately high. If the inlet vanes open too slowly, the pump might be unstable at first. Therefore, the operating speed should be chosen to correspond with a head that is considerably higher than Δh.

6.3 High level control summary

The proposed high level control concepts are summarised in this section and a schematic is shown in Fig. 34. The high level control receives a power setpoint $\hat{P}$, which is positive for turbine mode and negative for pump mode. Based on the measured head height Δh, it is verified if the system is able to operate at that power point. If this is not the case, the power setpoint is replaced with the closest viable power point $\hat{P}'$. Based on the power setpoint and head height, the lookup table interpolates between stored values, to output the speed setpoint $\hat{\Omega}_1$ and inlet vane angle setpoint $\hat{\alpha}$. Note that based on reservoir state, the lookup tables can switch between two lookup tables. In the first lookup table, Q is respectively minimal and maximal for turbine and pump mode. In the second lookup table, this is the other way around. Note that the stored output setpoints for rotational speed and inlet vane angle were calculated to reach the desired $\hat{P}$ at given Δh. However, since errors are present due to measurement error, modelling inaccuracies and interpolation, the output $\hat{\Omega}_1$ and $\hat{\alpha}$ will not reach $\hat{P}$ exactly. Therefore, a Perturb & Observe algorithm is used to complement the lookup table. Once the output parameters $\hat{\Omega}_1$ and $\hat{\alpha}$ of the lookup table are reached, the P&O algorithm makes small increments to $\hat{\Omega}_1$, while keeping $\hat{\alpha}$ constant. Doing this ensures that $\hat{P}$ is precisely reached. Combining the lookup table and P&O thus results in a highly dynamic, efficient and precise attainment of the power setpoint $\hat{P}'$. The rotational speed setpoint for the second runner is given by $\hat{\Omega}_2 = \zeta\ \hat{\Omega}_1$.

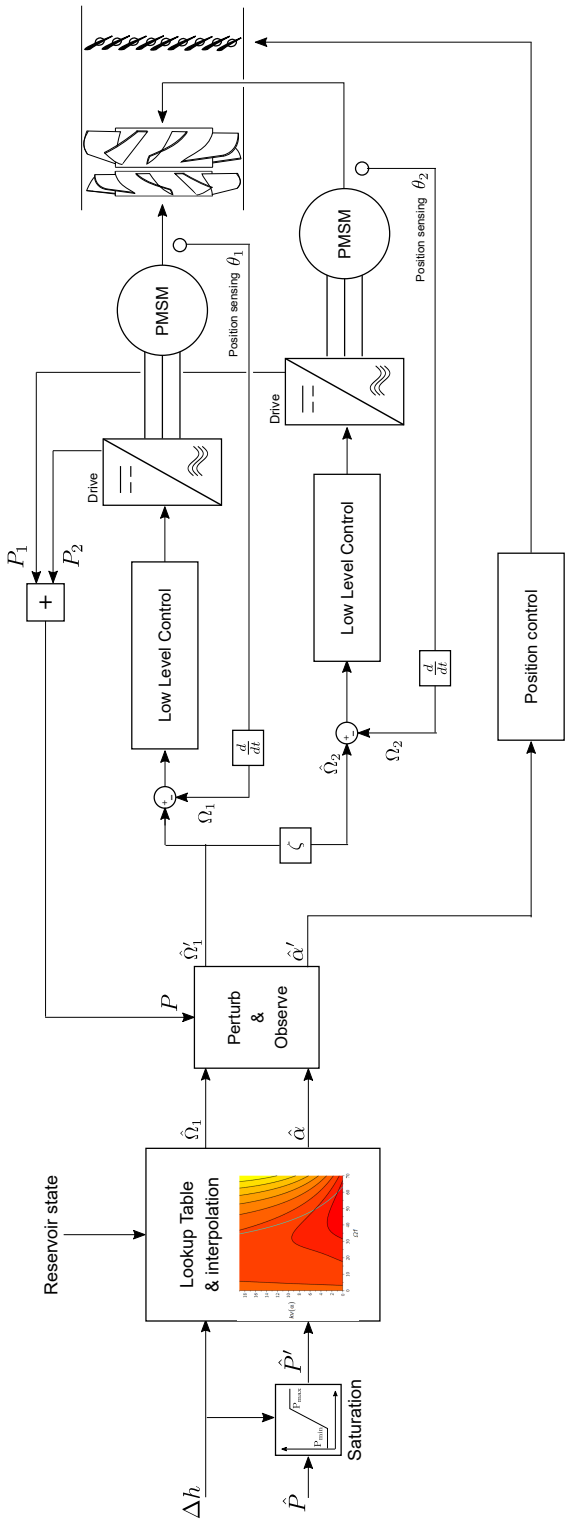

Figure 34: High level control schematic

7 Influence of a varying speed ratio

The effect of speed ratio variations has been simulated using CFD for a flow rate of $Q = 130$ m^3/s with variations of $\pm 5\%$. This ratio ζ is the ratio between the speeds of the second runner and the first runner and thus $\Omega_2 = \zeta \cdot \Omega_1$. In this section, the influence of the speed ratio and the viability of control systems with the extra control parameter Ω_2 are analysed.

7.1 Turbine

In turbine mode, the speed ratios of $\zeta = 0.85$ and $\zeta = 0.95$ were simulated for $\Omega_1 = 35$ rpm $-$ 60 rpm. However, the turbine is not stable for $\Omega_1 > 52$ rpm. Fig. 35 shows how turbine head h_{RPT} and power P_{RPT} change with different speed ratios. It can be seen that increasing or decreasing Ω_2 respectively decreases and increases head and power in the given ranges. This is the same effect as respectively increasing and decreasing Ω_1. Furthermore, it can be seen that the effect is significant. For a rotational speed of $\Omega_1 = 50$ rpm of the first runner, changing ζ from 0.85 to 0.9 to 0.95 gives a power of respectively $P = 6.1$ MW, $P = 5.0$ MW and $P = 3.7$ MW.

Since changing Ω_1 or Ω_2 has the same effect in the given region, Fig. 36 shows h_{RPT} and P_{RPT} vs. the mean rotational speed between both runners $\frac{\Omega_1+\Omega_2}{2}$ for the different speed ratios. Note that all points seem to follow the same curve. From this, it is clear that changing Ω_1 or Ω_2 has the same effect on head and power. Of course, this is only for ratios $0.85 - 0.95$ and where the turbine is stable. The analysis in section 6.1 can also be made for the mean rotational speed. Note that also a weighted mean rotational speed can be used, if this gives better uniform results. This enables the high level control to control an extra parameter and thus an extra degree of freedom. With this extra parameter, two extra constraints, that can be implemented, arise. Since the moment of inertia of the first runner $J_{r1} = 1.36 \cdot 10^5$ kgm^2 is lower than the second runner $J_{r2} = 2.07 \cdot 10^5$ kgm^2, the first runner can be accelerated or decelerated more quickly than the second runner. Therefore, by changing the rotational speed of the first runner faster, the mean rotational speed can also change faster than with a fixed ratio control system. In this control however, the ratio has to be within the limits of stability.

Fig. 37 illustrates the runner power lines vs. Ω_1 for different speed ratios. It can be seen that, especially for lower power points, there is a large discrepancy between P_r1 an P_{r2}. For $\Omega_1 = 50$ rpm and $\zeta = 0.9$, the power $P_{\mathrm{RPT}} = 5.0$ MW (see Fig. 35b). This power is split into $P_{r1} = 0.8$ MW and $P_{\mathrm{RPT}} = 4.2$ MW. To reach 5 MW with $\zeta = 0.85$, $\Omega_1 \approx 51$ rpm. Here, $P_{r1} \approx 0.5$ MW and $P_{r2} \approx 4.5$ MW. To reach 5 MW with $\zeta = 0.95$, $\Omega_1 \approx 48$ rpm. Here, $P_{r1} \approx 1.2$ MW and

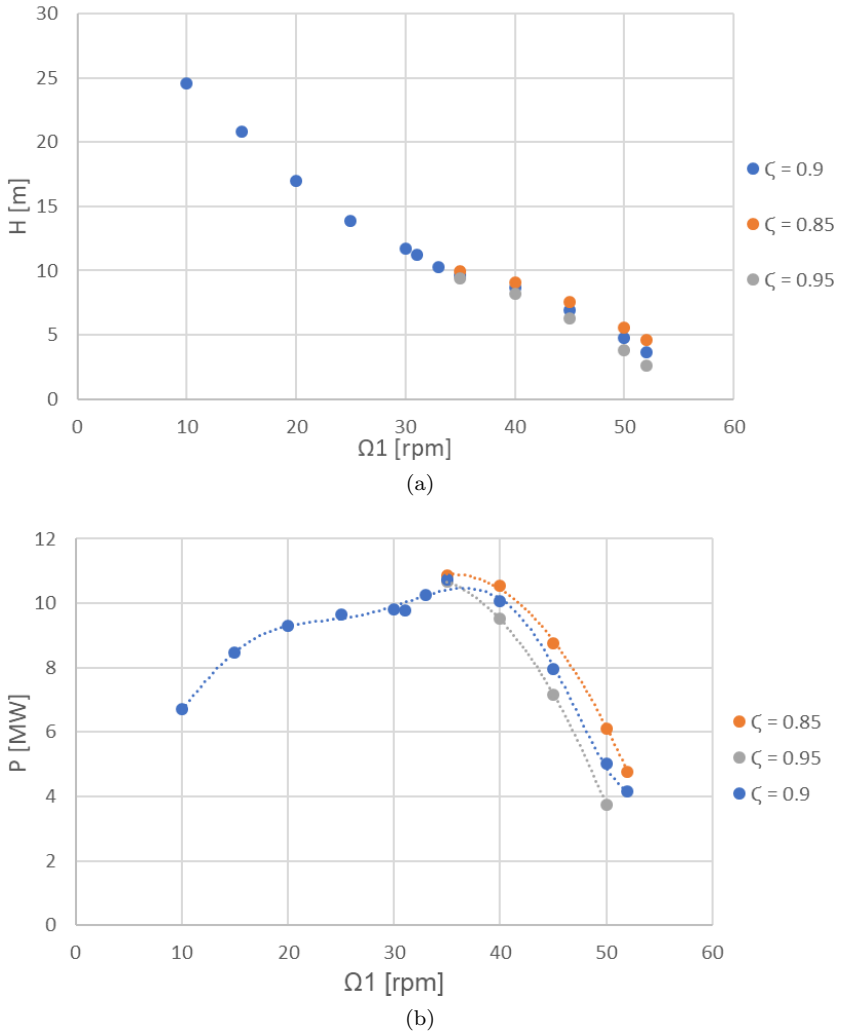

Figure 35: (a) Turbine head H_{RPT} and (b) Turbine power P_{RPT} versus Ω_1 for speed ratios of 0.95, 0.9 and 0.95

$P_{r2} \approx 3.8$ MW. It can be concluded that using a variable speed ratio, the same power can be reached, but with a different power share between both runners. In the control system, next to the possibility of using the ratio to increase dynamics and power response time, there can be opted to use this ratio control to e.g. let the power vs. nominal power ratio of both runners be equal. This of course depends on the nominal power of both electrical machines.

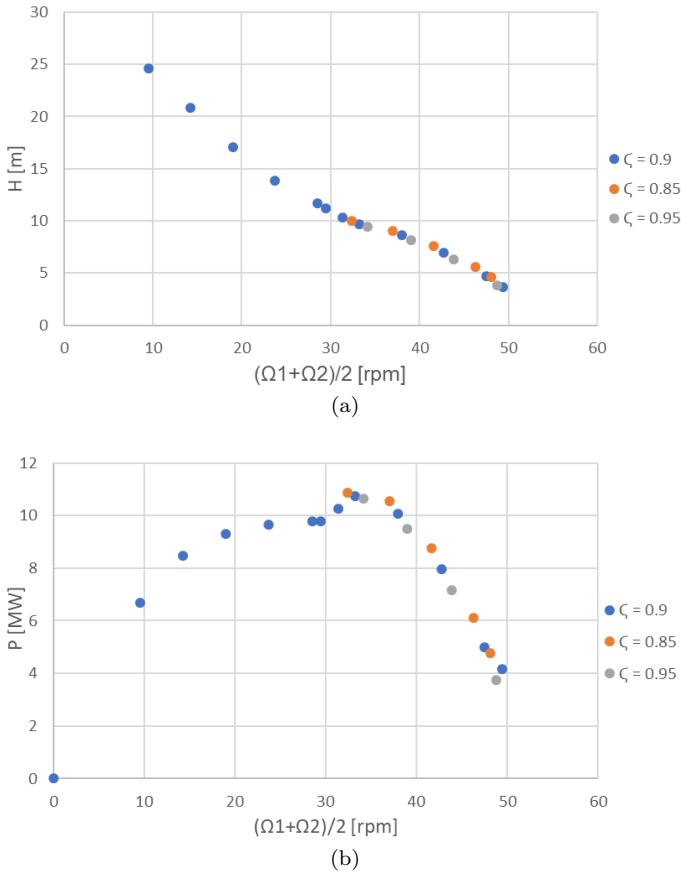

Figure 36: (a) Turbine head H_{RPT} and (b) Turbine power P_{RPT} versus $\frac{\Omega_1+\Omega_2}{2}$ for speed ratios of 0.95, 0.9 and 0.95

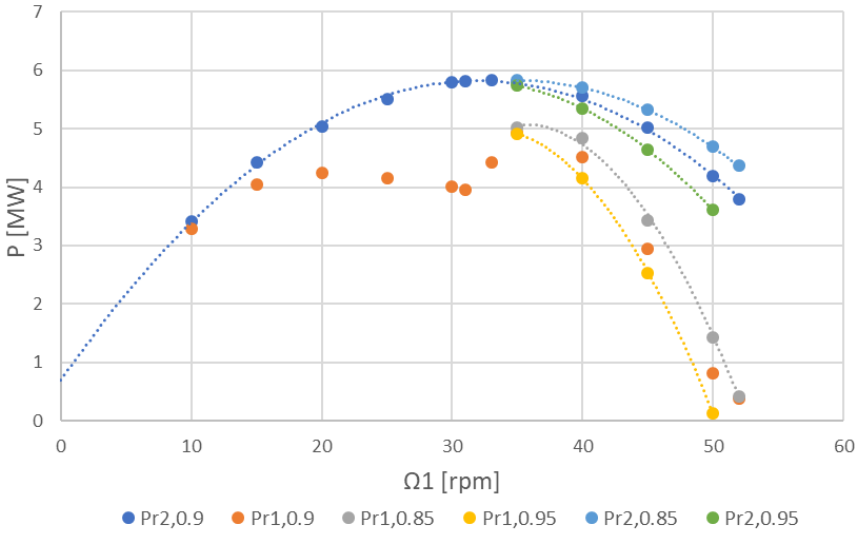

Figure 37: P_{r1} and P_{r2} versus Ω_1 for speed ratios of 0.95, 0.9 and 0.95

7.2 Pump

For pump operation, the same analysis is executed as for turbine mode. Also for the pump characteristics at ±5%, the analysis can be done for a (weighted) mean rotational speed. Therefore, the same control concepts apply in pump mode. The most notable difference between the influence of speed ratio in pump mode, compared to turbine mode, is that the power of the first runner's power doesn't change with varying ratio. This can be seen in Fig. 40. Therefore, unlike in turbine mode, the ratio between the runner powers does not behave the same as the ratio between the runner speeds. Controlling both runners to work at a certain percentage of nominal power is still possible, but is less straightforward to implement.

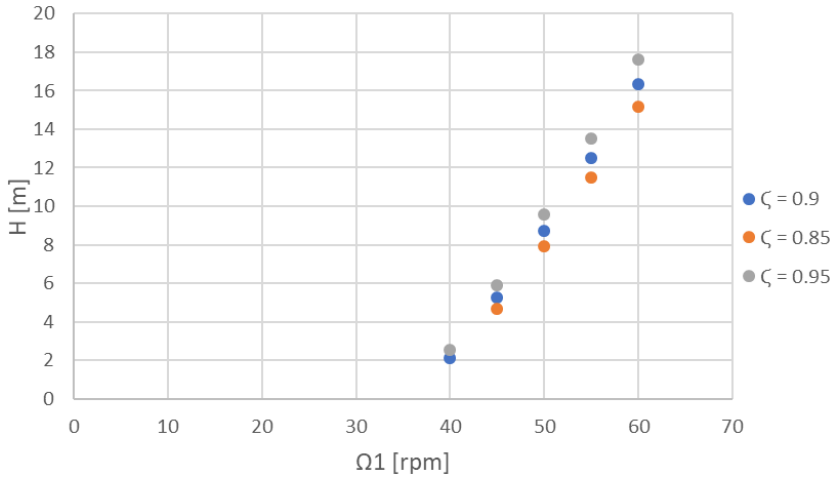

(a)

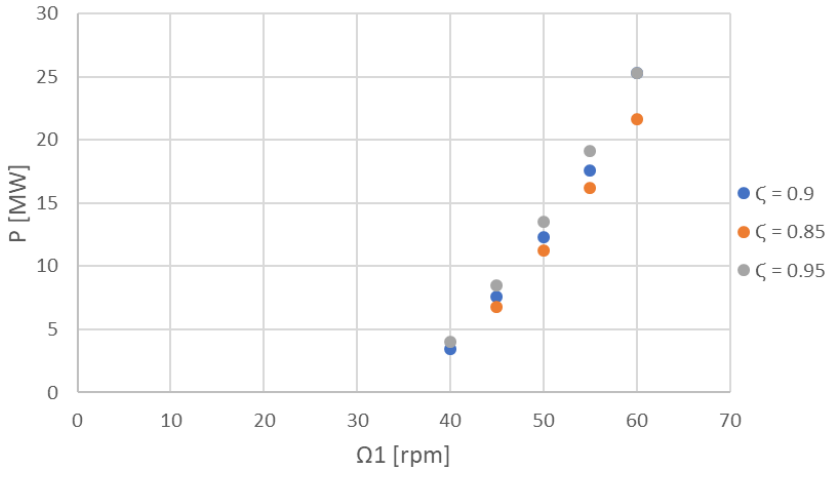

(b)

Figure 38: (a) Pump head H_{RPT} and (b) Pump power P_{RPT} versus Ω_1 for speed ratios of 0.95, 0.9 and 0.95

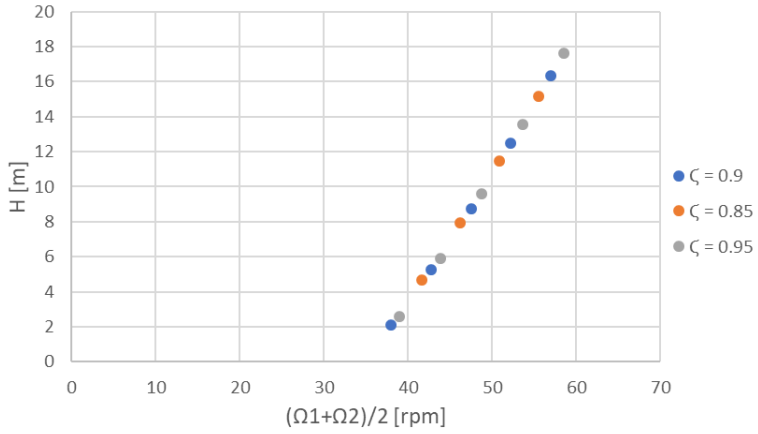

(a)

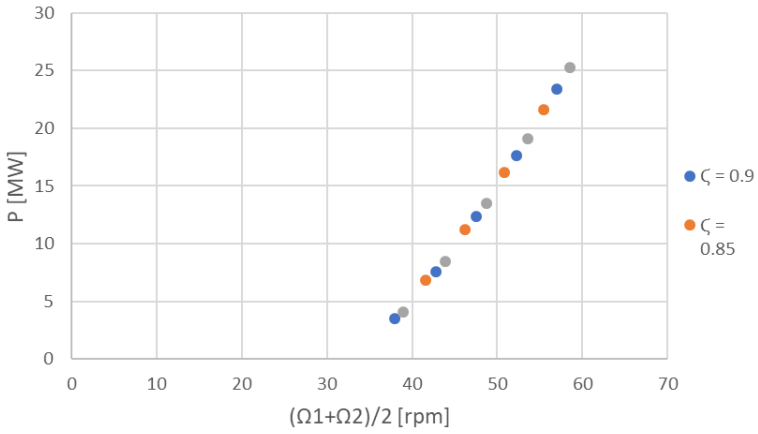

(b)

Figure 39: (a) Pump head H_{RPT} and (b) Pump power P_{RPT} versus $\frac{\Omega_1+\Omega_2}{2}$ for speed ratios of 0.95, 0.9 and 0.95

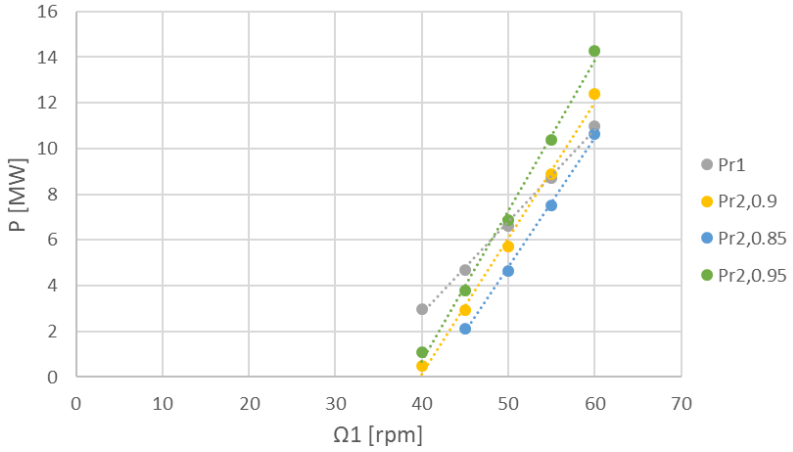

Figure 40: P_{r1} and P_{r2} versus Ω_1 for speed ratios of 0.95, 0.9 and 0.95

8 Positive displacement RPT

Aside from the shaft- and rim-driven RPT concepts, the positive displacement (PD) RPT is also under consideration in the ALPHEUS project. Fig. 41 shows a cross section of this RPT concept [5]. The RPT consists of two contra-rotating lobes, forcing the water flow in one direction in pump mode, or driven by the water flow in the reverse direction in turbine mode. As previously discussed, the shaft- and rim-driven RPT concepts require a regulation of the relative speed ratio between the two runners to maximize efficiency and control dynamics. In contrast, the positive displacement RPT requires an accurate regulation of the relative position of the lobes to avoid collision. The gap between the lobes must be regulated at a fixed and narrow distance, e.g., 20 mm. A collision would cause severe damage and immediate failure of the system. Hence, the main difference between the shaft- and rim-driven RPT's on the one hand and the positive displacement RPT on the other hand is that the challenge of kinematic coordination lies in accurate control of relative position instead of speed. A speed mismatch results in a reduced efficiency for the shaft- and rim-driven RPT's, while a position mismatch results in damage and failure for the positive displacement RPT. Aside from the relative position control, the system must also be variable in speed to be able to regulate the power, both in turbine and pump mode. The control challenge is thus two dimensional, i.e., both the speed must be controlled and the relative position of the lobes must be ensured.

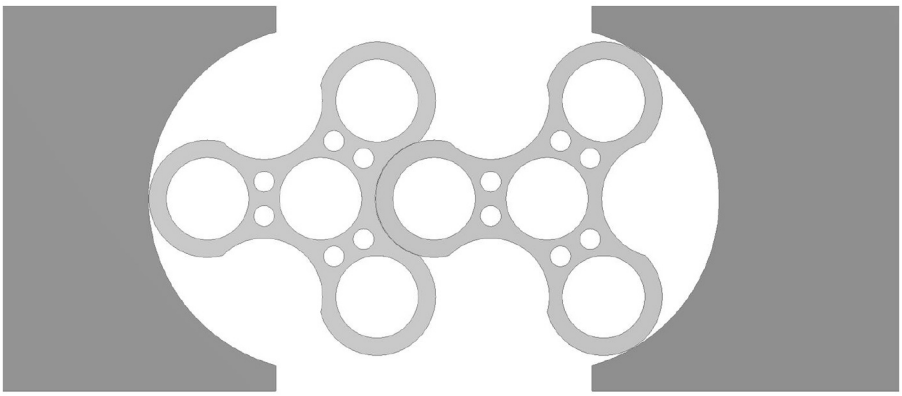

Figure 41: Positive displacement RPT concept by Ronamic [5]

The relative position control can be realised mechanically and electrically. The mechanical solution would be to use two gears and one PMSM as motor/generator, while the electrical solution would use two separate PMSM's in combination with an accurate position control via the machine torques. The mechanical solution is often used in screw compressors and is simple & robust. However, mechanical gears are not straightforward to use on the high envisioned power level of 10MW. Also, they introduce friction, and thus mechanical losses, that reduce the overall efficiency of the system. For these reasons, the electrical solution is certainly

appealing, but requires further analysis and study in simulation models to investigate whether the accurate relative positioning requirements can be reached, also in dynamic conditions.

An additional challenge is that the torque of the lobes contains a large torque ripple. Based on the design of the RPT, it can indeed be expected that the lobes cause a pulsating torque. Fig. 42 shows a simulation result clearly showing the oscillations in torque and power [5].

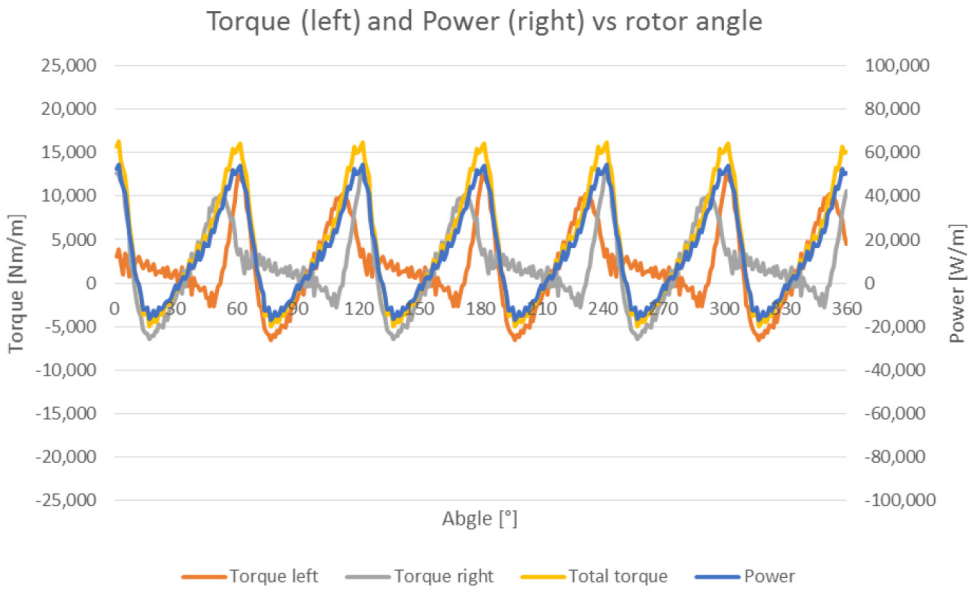

Figure 42: Torque ripple for the positive displacement RPT [5]

Fig. 44 schematically shows the control system envisioned for the PD RPT in ALPHEUS. The power setpoint $\hat{P}$ is the input of the control system on the top left. The power controller determines a speed setpoint $\hat{\Omega}_1$ for the primary rotor based on a high level control algorithm cfr. the control of the shaft- and rim-driven RPT's. A cascaded speed and torque control system, respectively using a PI and a Field-Oriented Controller, then ensures the realisation of this speed setpoint. The secondary control system at the bottom regulates the relative position difference to zero, i.e., $\theta_1 - \theta_2 = 0$. This is realised by a cascaded speed, position and torque control. Intermediate feedforwards are foreseen to improve the control performance by means of system knowledge of, e.g., inertia, friction, etc.

Since limited CFD calculations are available for now, a detailed analysis for the high level control for the PD RPT is not included in this deliverable. However, Fig. 43 shows a turbine characteristic for a small scale model at $\Delta h = 2$ m [5]. It can be seen that the turbine curves have the same form as for the CR RPT types. Therefore, the high level control concepts, discussed in this deliverable, are presumably also relevant for the positive displacement RPT. A future research step

in ALPHEUS is to implement this control system including a dynamic model of the RPT and mechanical dynamics. An important aspect to include in this model is the strong pulsating torque as shown in Fig. 42, as this poses a considerable difficulty to regulate the relative angle of the lobes in dynamic conditions. If it turns out to be infeasible to regulate the gap between the lobes with sufficient accuracy due to this pulsating torque, it will be investigated whether additional inertia, e.g., flywheels, can be added to stabilize the relative position control.

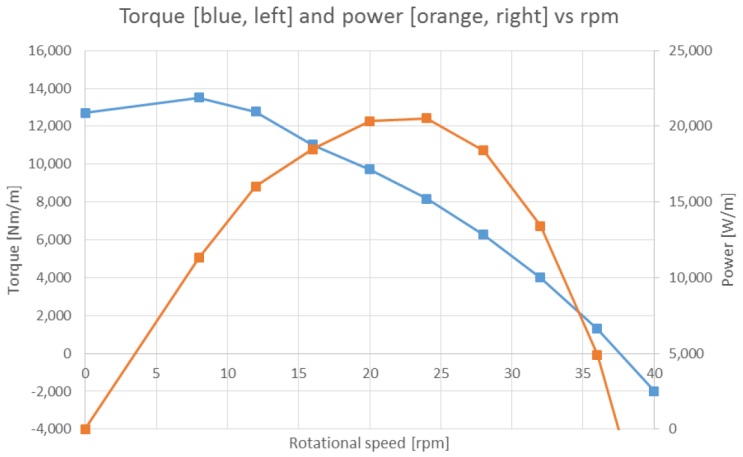

Figure 43: Torque (blue) and Power (red) vs. Ω_1 in turbine mode for $\Delta h = 2$ m [5]

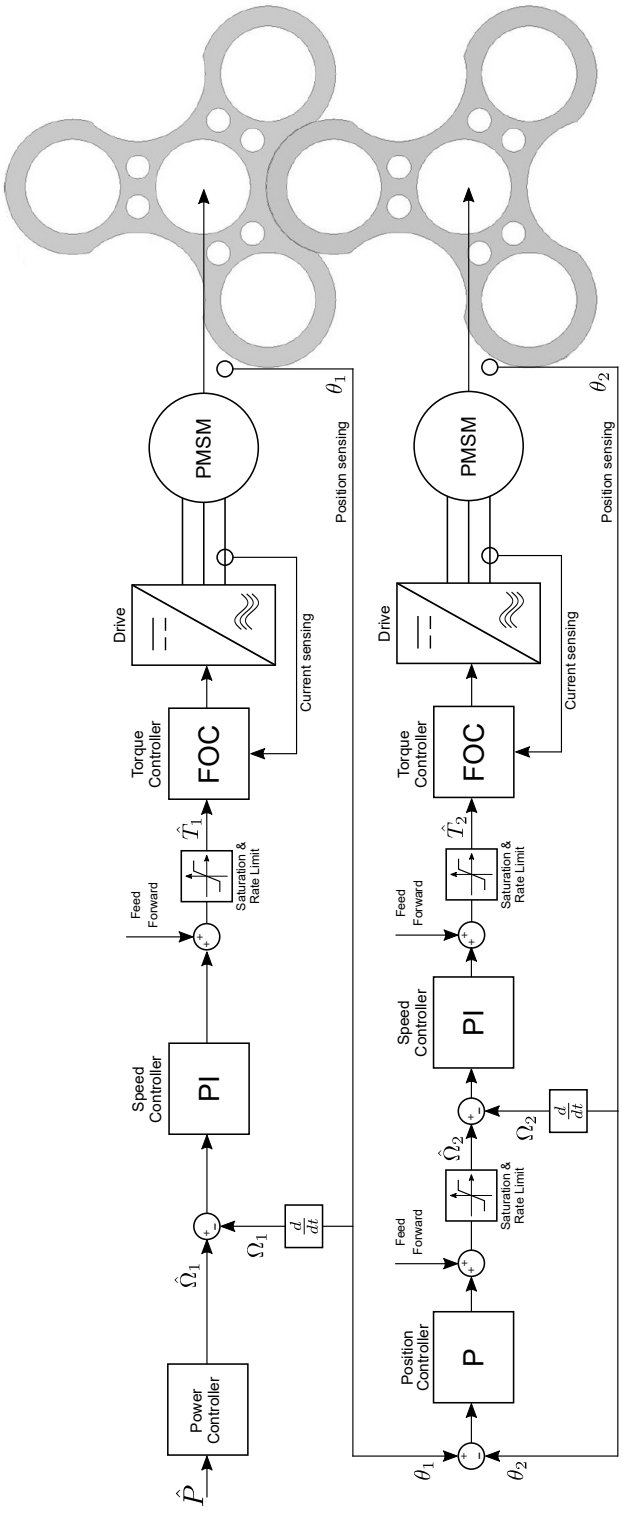

Figure 44: Control system for the positive displacement RPT

Appendices

A Derivation of flow rate from energy conservation

Throughout this section, a number of assumptions will be made. These assumptions include:

- Steady and incompressible flow
- No reservoir pressure difference or head change
- Constant tube diameter
- Wholly turbulent flow

A.1 Law of conservation of energy

The law of conservation of energy for a steady & incompressible flow in a certain control volume is given below, where h_L is combination of major and minor losses, expressed as a head loss. h_p is the power added to water (pump mode) and h_t is the power extracted from the water steam (turbine):

$$\dot{m}\left(\frac{p_{\text{in}}}{\rho}+\frac{v_{\text{in}}^2}{2}+g(h_{\text{in}}+h_p)\right) = \dot{m}\left(\frac{p_{\text{out}}}{\rho}+\frac{v_{\text{out}}^2}{2}+g(h_{\text{out}}+h_L+h_t)\right) \tag{32}$$

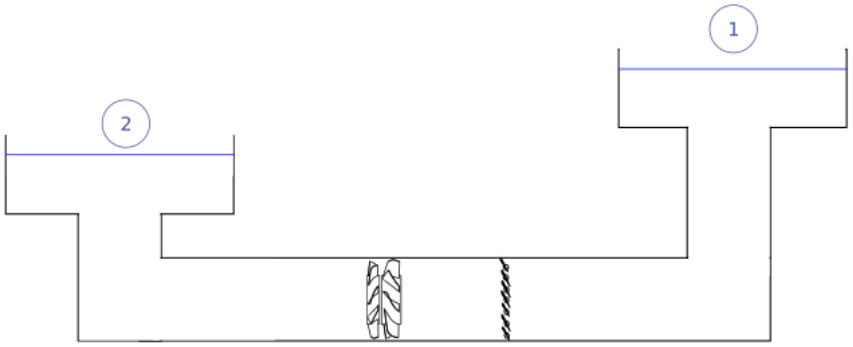

Figure 45: Simplified principle of ALPHEUS water model

For a mass flow from upper to lower reservoir, relating to a flow from 1 to 2 as given in Fig. 45, p_{in} corresponds with p_1, p_{out} with p_2 and so on. On the contrary, for a flow in opposite direction (from 2 to 1) p_{in} and p_{out} correspond with respectively p_2 and p_1. Furthermore, point 1 and point 2 were chosen to be on top of the reservoirs. Both points are open to the atmosphere ($p_1 = p_2 =$

p_{atm}) and the velocities at both locations are negligible, due to the large reservoir surfaces ($v_1 = v_2 = 0$). Therefore, the equations for downstream (with turbining) and upstream (with pumping) flow respectively become:

$$|\dot{m}|g(h_1) = |\dot{m}|g(h_2 + h_L + h_t) \quad (33)$$

$$|\dot{m}|g(h_2 + h_p) = |\dot{m}|g(h_1 + h_L) \quad (34)$$

Both equations can be combined into one equation, by choosing $\dot{m}$ to be positive when the flow direction is from point 1 to point 2, and thus, downstream:

$$\dot{m}\ g\ h_{\mathrm{RPT}} = \dot{m}\ g\ (h1 - h_2) - |\dot{m}|\ g\ h_L \quad (35)$$

Since the goal is to find an equation for water flow Q, $\dot{m}$ is replaced by $Q \cdot \rho$. $h_1 - h_2$ is written as Δh:

$$|Q|\ \rho\ g(\Delta h - h_{\mathrm{RPT}}) = \rho\ g\ Q\ h_L \quad (36)$$

As will be further discussed, h_L and h_{RPT} are a function of a.o. Q, so (36) can be rewritten as:

$$|Q|\ \rho\ g(\Delta h - h_{\mathrm{RPT}}(Q)) = \rho\ g\ Q\ h_L(Q) \quad (37)$$

A.2 Modelling the head losses

A.2.1 Major losses

Major losses comprise the flow resistance due to friction with the tube walls. This can be expressed as the sum of the flow resistance of all tubes, where tubes of different diameters might be used. According to the Darcy-Weisbach Formula:

$$h_{L,M} = \sum_i f_i \frac{L_i}{D_i} \frac{v_i^2}{2g} = \sum_i f_i \frac{L_i}{D_i} \frac{\left(\frac{Q}{A_i}\right)^2}{2g} = \sum_i f_i \frac{8\ L_i}{\pi^2\ D_i^5} \frac{Q^2}{g} \quad (38)$$

Here, f_i is the friction factor of each tube and is dependent on the Reynolds number Re of the flow and the relative roughness $\frac{e}{D}$ of the tube, where e is the mean height of the imperfections on tubes' surfaces. If both are known, f_i is found from the Moody diagram, as shown in Fig. 46. Haaland's formula gives an explicit empirical formula to define f_i, although it's not as accurate as the Moody diagram.

$$\frac{1}{\sqrt{f_i}} \simeq -1.8 \log\left(\frac{6.9}{Re_i} + \left(\frac{e_i/D_i}{3.71}\right)^{1.11}\right) \quad (39)$$

If $Re \cdot \frac{e}{D} > 560$ the flow inside the tube can be classified as wholly turbulent.

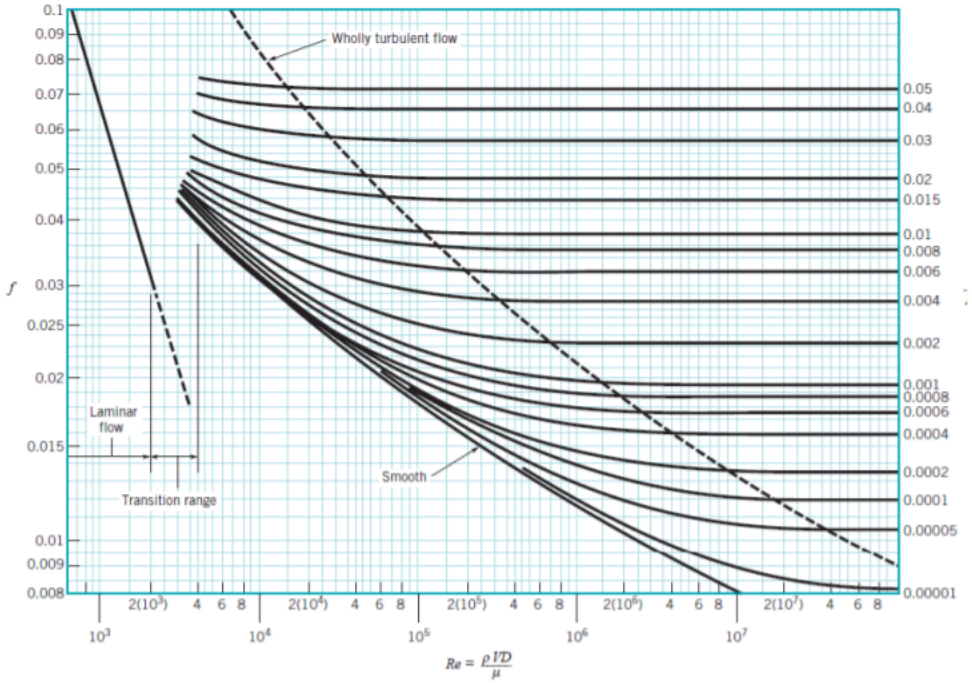

Figure 46: Moody diagram [1]

The friction factor depends only on the relative roughness and can be expressed as:

$$f_i = \frac{1}{(2\ \log\frac{D}{e} + 1.138)^2} \tag{40}$$

Whether (39) or (40) should be used, depends on parameter e for the tubes that will be used in our system. Quick estimates show that if e is larger than 5 mm, (40) should be used. For the system in Fig. 45, where the tube diameter is constant, substitution of (40) in (38) gives:

$$h_{L,M} = \frac{1}{(2\ \log\frac{D}{e} + 1.138)^2} \frac{8\ L}{\pi^2\ D^5} \frac{Q^2}{g} \tag{41}$$

A.2.2 Minor losses

Minor losses include all local flow losses due to valves, elbows, expansions and other local objects restricting flow.

$$h_{L,m} = \sum_i k_i \frac{v_i^2}{2g} = \sum_i k_i \frac{8}{\pi^2 D_i^4} \frac{Q^2}{g} \tag{42}$$

In this equation, k_i is the coefficient of minor loss and can be found in tables such as table 47. In this document, the minor losses for the inlet vanes are the most important, as these vanes are one of the control parameters used to alter the flow, and thus regulate the system. As shown in table 47, the variable minor loss coefficient for the inlet vanes k_v can be determined for different opening states from available tables. Through these points, a curve can be derived to have a continuous equation in function of the vane angle or opening. The equation for the inlet vanes losses becomes:

$$h_{L,v} = k_v(\alpha)\frac{8}{\pi^2 D^4}\frac{Q^2}{g} \tag{43}$$

Figure 47: Minor losses coefficients for valves in different opening states [2]

No	Type of valve	A coefficient of minor loss
1	Globe valve, fully open	10
2	Angle valve, fully open	2
3	Gate valve, fully open	0,15
4	Valve gate, ¼ closed	0,26
5	Gate valve, ½ closed	2,1
6	Gate valve, ¾ closed	17
7	Fully open ball valve	*0,05*
8	Gate valve, ⅓ closed	5,5

From table 47, we can fit a curve between the values for a gate valve. Additionally to the given operating points, we know that there is no flow when the gate is fully closed ($\alpha = 1$) and thus $k_v(1) = \infty$.

$$k_v = \frac{-1348/75\ \alpha^3 + 41/5\ \alpha^2 - 128/75\ \alpha}{\alpha - 1} \tag{44}$$

A.3 Derivation of the flow rate

Combining (36), (41), (42) and (43) for a system with constant diameter gives:

$$\begin{aligned}&\operatorname{sgn}(Q)Q\rho g(\Delta h - h_{\mathrm{RPT}}(Q)) = \\ &Q\rho g\left(\frac{L}{(2\ \log\frac{D}{e} + 1.138)^2\ D} + k_v(\alpha) + \sum_i k_i\right)\frac{8}{\pi^2\ D^4}\frac{Q^2}{g}\end{aligned} \tag{45}$$

Simplified this becomes:

$$\operatorname{sgn}(Q)\cdot Q^2 = \frac{\pi^2\ D^4\ g\ (\Delta h - h_{\mathrm{RPT}}(Q))}{8\ (k_c + k_v(\alpha))} \tag{46}$$

$$k_c = \frac{L}{(2\ \log\frac{D}{e} + 1.138)^2 \cdot D} + \sum_i k_i \tag{47}$$

B Vector control

The general concept behind vector control is to regulate the currents i_d and i_q as constant values in the rotating reference frame. i_d and i_q can be calculated from the phase currents i_a, i_b and i_c through the Clarke-Park transform. Fig. 48 gives a schematic representation of the PMSM. The stator is represented by three windings a, b and c while the rotor is shown as a magnet with a rotating d and q axis. The rotor is represented schematically with a single pole pair for simplicity, although the following analysis is valid for any pole pair number . The permanent magnet flux is directed along the d axis. This causes a back-emf in the q-axis, as the back-emf equals the derivative of the magnet flux. Therefore, its phasor lags 90°behind.

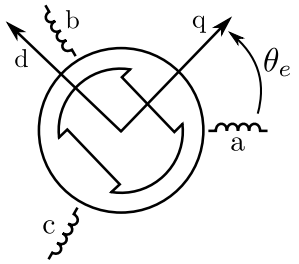

Figure 48: Definition of the reference axis in a PMSM

Fig. 49 shows the equivalent scheme of the PMSM in the rotating reference frame. The reference direction of the currents is chosen towards the machine, i.e., corresponding to motor operation. The scheme remains equally valid for generator operation, but currents will be negative. The q scheme contains the back-emf of the permanent magnets Ω_e in series with the armature reaction emf $\Omega_e L_d i_d$, the q axis inductance L_q and the stator resistance. The d scheme contains the armature reaction emf $-\Omega_e L_q i_q$, the d axis inductance L_d and the stator resistance. It is important to note that the q axis current affects the d axis scheme and vice versa through the armature reaction voltages. Therefore, the q and d schemes are coupled.

By regulating the d and q axis currents, the torque can be regulated, as shown in the general torque equation of the PMSM:

$$T = N_p \frac{3}{2} \left[\Psi_{\mathrm{PM}} i_q + (L_d - L_q) i_d i_q \right] \tag{48}$$

Here, N_p is the pole pair number, Ψ_{PM} is the constant flux of the permanent magnets, L_d and L_q are the d and q axis inductances respectively. i_d and i_q are the d and q axis currents. Torque control using FOC requires the use of current sensors to measure the machine currents, and a position sensor (encoder or resolver) to measure the rotor position θ. Fig. 50 shows the general control

scheme of a vector controlled PMSM. At the bottom right, the measured currents i_a, i_b and i_c are converted to q and d components i_q and i_d using a Clarke-Park transformation. To perform this transformation, the rotor angle θ must be known, hence the position measurement. Not all three stator currents need to be measured, since the neutral wire is not connected, so the sum of the currents must be zero. Therefore, measuring two currents is sufficient. The measured q and d axis currents are compared with current setpoints $\hat{i}_q$ and $\hat{i}_d$ by two PI controllers. The PI controllers determine the duty ratios of the converter, after transformation to the stationary reference frame. These signals are finally sent to the PWM modules to determine the switching signals of the converter. Classically, PI controllers are used here, not P, as the integral action is crucial to avoid a steady state error. A derivative D action is avoided as it amplifies noise, which is a justified concern when measuring currents at a high frequency in a noisy environment.

This control concept is denoted 'vector control', as the torque is controlled by regulating the current vector i in the rotating reference frame. By following the setpoints $\hat{i}_q$ and $\hat{i}_d$, the current vector is controlled in both modulus and angle, with respect to the rotating rotor. It is important to note that there are two degrees of freedom, the q and d axis current, to regulate one single quantity, i.e., the torque. There are multiple ways of dealing with this additional degree of freedom, as will be explained in what follows. The strength of vector control lies in the fact that the torque can be regulated without the necessity of a torque measurement. The torque is controlled based on current control instead. Current is far easier and cheaper to measure compared to torque. Moreover, current can be measured at a high frequency with sufficient precision, which is not the case for torque measurement.

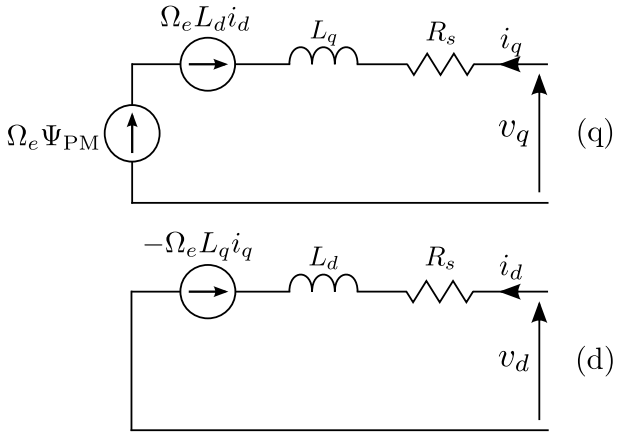

Figure 49: Equivalent schemes of a PMSM in a rotating reference frame

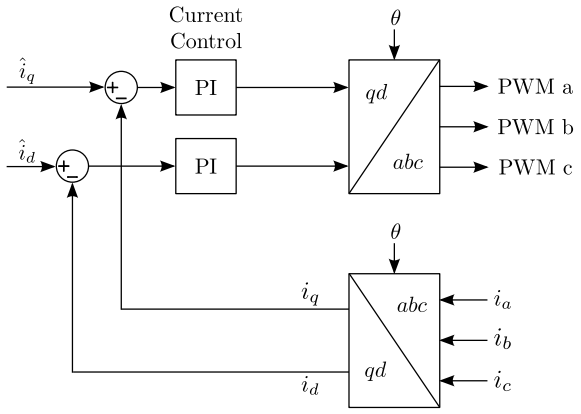

Figure 50: Vector control of a PMSM

References

[1] K. Al-Astal, A. Al-Agha, R. Awad, "Water Flow in Pipes," [Online]. Available: http://site.iugaza.edu.ps/mnazli/files/2017/02/Hydraulics-Discussion.pdf

[2] Z. Lubis, T. Manik, M. Rinkanto, T. Sitorus, "Design of a heat exchanger of three concentric tube layer on contrary flow," in *IOP Conference Series: Materials Science and Engineering. 505. 012091.* (2019) doi: 10.1088/1757-899X/505/1/012091.

[3] Engineering ToolBox, (2004). "Minor or Dynamic Loss Coefficients for Pipe or Tube System Components," [online]. Available: https://www.engineeringtoolbox.com/minor-loss-coefficients-pipes-d_626.html

[4] L. Nelik, "Stable and Unstable Pump Curves", Pumps & Systems [Online]. Available: https://www.pumpsandsystems.com/stable-and-unstable-pump-curves

[5] ONE Simulations BV, "RONAMIC Pump and Turbine - CFD simulations turbine performance", 2016-10-19.